Final Report on

Microstructure Sensitive Design and Processing in Solid Oxide Electrolyzer Cell

By: Dr. Hamid Garmestani

School of Materials Science and Engineering

Georgia Institute of Technology

June 12th, 2009

SUMMARY

The aim of this study was to develop an inexpensive manufacturing process for deposition of functionally graded thin films of LSM oxides with porosity graded microstructures for use as IT- SOFCs cathode. The spray pyrolysis method was chosen as a low-temperature processing technique for deposition of porous LSM films onto dense YSZ substrates. The effort was directed toward the optimization of the processing conditions for deposition of high quality LSM films with variety of morphologies in the range of dense to porous microstructures. Results of optimization studies of spray parameters revealed that the substrate surface temperature is the most critical parameter influencing the roughness and morphology, porosity, cracking and crystallinity of the film. Physical and chemical properties of deposited thin films such as porosity, morphology, phase crystallinity and compositional homogeneity have shown to be extensively dependent on the preparation conditions. Detailed analysis of the film formation mechanisms have been discussed in this work. It is suggested that using volatile metal-organic precursors as in CVD would alter the film formation mechanism to MOCVD process in which films of high quality can be processed. Novel electrode microstructures currently include a graded microstructure wherein the large pores are made close to the surface in outer layers for maximum mass transport into the electrode structure and smaller pores and particles close to the electrolyte interface would create maximum number of active reaction sites. Taking the advantage of simplicity of spray pyrolysis technique combined with using metal-organic compounds, the conventional ultrasonic spray system was upgraded to a novel system whereby highly crystalline multi-

layered porosity graded LSM cathode with columnar morphology with good electrical conductivity in the range of 500-700 °C was fabricated through a multi-step spray and via optimizing spray parameters. This achievement for the current graded LSM cathode would allow its use in IT-SOFCs.

CHAPTER 1

INTRODUCTION

1.1 Research Objectives and Motivation

The desire for decreasing dependence on petroleum supplies and lowering environmental contaminations has turned nations' strategies towards rapid development of alternative high efficiency energy technologies. Interest in developing higher efficiency and environmental friendly energy/power generation has particularly led to pursue extensive research on development and commercialization of electrochemical energy storage and converter systems such as capacitors, batteries and fuel cells. Among these systems, fuel cells have shown to be promising alternative resources in efficient and low emission power generation and are expected to solve traditional energy supply issues for the next generation. Basically, fuel cells are the electrochemical engines that convert the same chemical energy as in combustion engines directly into electrical power with higher efficiency and low pollution. In addition to that, the waste heat from a fuel cell can be utilized to boost the entire system efficiency. Other benefits of the fuel cells associated to the environment include production of pure water out of the chemical process and that they can operate silently.

Solid oxide fuel cells (SOFCs) are solid-electrolyte types of fuel cells with unique capability of being economically competitive to other fuel cell due to having highest power density, fuel versatility, variety of cell configurations and no need for using expensive metal catalysts. These advantages are associated with high operating temperature (700-1000 °C) of the SOFC and the ceramic nature of all components which also inevitably posses some major problems towards commercialization of the SOFC

technology. Cost and durability are currently the main challenges in designing optimized structures of SOFCs for the entire range of possible applications in stationary, transport and portable power generation. One possible solution is lowering the operating temperature of the SOFC to intermediate temperature (500-750 °C) that would allow using much less expensive materials in the entire cell construction and as a result lead to significant drop in cost and increasing life of the SOFC technology. Designing intermediate temperature solid oxide fuel cells (IT-SOFCs) is therefore one of the important objectives that is being pursued in current researches. For instance, thermal mismatch between components due to different high temperature thermal coefficient of expansion (TCE) of the components, chemical instability of the materials at the interfaces and sintering of electrode particles over time make reduction of the operating temperature of the SOFC desirable to mitigate the technical issues associated with elevated temperatures. However, moving to lower operating temperatures is on the other hand, the origin of some critical problems in functionality of the cell components. $La_{1-x}Sr_xMnO_3$ perovskite (LSM) is regarded as one of the most promising cathode materials for SOFCs due to its high thermal and chemical stability particularly with yttrium stabilized zirconia (YSZ) electrolyte [1-5]. The main problem arises when lowering the temperature results in increasing polarization resistances between LSM cathode and YSZ electrolyte. [6]

Extensive research has been focused so far on finding ways to overcome problems associated with low temperature of operation in SOFCs.

Materials design approach has been applied for development of high performance viable IT-SOFCs and to process materials with improved electronic and thermal properties. The ABO_3 perovskite structured oxides used as the SOFC cathode, allow for

selective substitution of cations in different valence states within A and B sites as well as relatively high concentration of vacancies in the oxygen sublattice, without significant changes of the perovskite structure. Many perovskite oxides (e.g. SCFN and LSCF) have been studied and developed as the mixed ionic and electronic conductors (MIEC) that can provide the path for transferring both electrons and ions to improve the electrochemical performance of the IT-SOFCs cathode [7-14]. Moreover, recent studies have shown the potential of some perovskite related structures such as $GdBaCo_2O_{5+\delta}$ and $SmBaCo_2O_{5+x}$ with layered and doubled structures, respectively, for operation at reduced temperatures due to their low activation energy. This trend has still some drawbacks, as some properties may change in the undesirably while others are improved; for example, lanthanum strontium cobaltite (LSC) shows high electrical and ionic conductivity at low temperature compared to LSM, however, its TCE is much higher than those of typical SOFC electrolytes [15-18]. Fabrication of composite cathodes has also demonstrated to be an effective way of increasing triple phase boundaries (TPB) between cathode, gas and the electrolyte. LSM–YSZ and LSM–CGO are well-known composite cathodes that have been extensively studied [19-24].

Another approach is to improve the microstructure such that it compensates for issues that would result in the performance losses associated with lower operating temperature. This approach necessitates design of manufacturing processes that allow tailoring the microstructure to achieve desirable properties via controlling and optimization of processing parameters. Novel fabrication techniques have been developed that demonstrate variety of advantages over other methods [25]. However, few attempts have been made to develop processing techniques that are capable of cost effective and

large scale manufacturing of functional, porous, and nanostructured electrodes with improved properties. The cathode microstructure has been recognized as one of the most important factors determining the performance of the SOFC, since the electrochemical performance and thermal stability of SOFC depend basically on the chemical composition and morphology of the electrode. High mixed conductivity, chemical and thermal expansion compatibility, better resistance to sintering creep and failure, and high specific surface area are among critical properties of cathode electrodes that need to be obtained at the same time under working conditions. The cathode microstructure requires adequate porosity for oxygen supply and transport while providing electrochemical reaction sites for oxygen reduction as well as a path for electrons to be transported from the cathode/electrolyte reaction sites to the surface of the cathode. Therefore, to achieve a balance between these two conflicting requirements for charge and mass transfer, graded electrode structures with a finer microstructure and porosity close to the electrolyte and coarser microstructure and larger porosity away from it has to be developed [26, 27]. Recently, microstructure sensitive design (MSD) has been applied to propose a multi-scale model -based on statistical continuum mechanics-for the cathode electrode with optimized electrical and mechanical properties. According to this model, a gradient porous microstructure with a fine microstructure layer close to the surface of the electrolyte and a coarse outer layer is expected to show more compatibility of properties in different layers [28-30].

Functionally graded materials (FGMs) approach has been applied to SOFCs components to incorporate advantages of compositional or microstructural variations such as porosity in some spatial direction into component design to improve the

functionality of individual layers at low temperatures [31-33]. Theoretical analysis of the graded composite cathodes indicates that composition grading could improve transport properties through the electrode at low operating temperature and enhance the electrochemical performance of the cell. Most of the analysis reported in the literature is performed on compositionally graded LSM–YSZ cathodes [34]. In some of the proposed models, the porosity gradient through the cathode layer is also incorporated [26, 32, 35-37]. It is of great interest that the grading will reduce the coefficient of thermal expansion (CTE) mismatch between the electrode and the electrolyte substrate resulting in improvement of adhesion, durability and mechanical stability of the cell components.
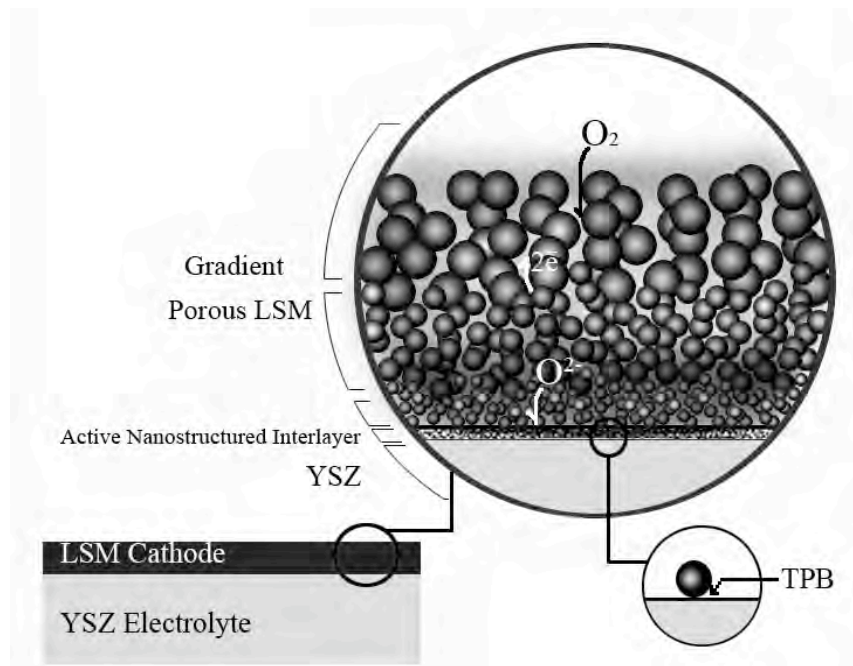

Fig. 1.1. Schematic of a functionally graded porous LSM cathode on YSZ substrate. Large spheres represent large particles creating large columnar pore structure in the outer layer to allow gas transport. Spheres gradually get smaller along the inner layers to maintain the structural integrity. Small spheres and the small pores close to the electrolyte maximize the number of triple phase boundary (TPB) in the active nanostructured interlayer.

In order to achieve almost all cathode requirements and properties at the optimum level and also for the gas diffusion to be not rate limiting, 20-30% porosity is assumed to

be required [34, 38, 39]. Fig. 1.1 shows the schematic of the proposed functionally graded porous LSM cathode which consists of large particles and the columnar pore structure in the outer layer to allow the gas in from the surface. The particles and the pores gradually get smaller toward the electrolyte to maximize the number of triple phase boundary (TPB) in the active nanostructured interlayer.

Having all advantages, there are few reports on the potential processing techniques for manufacturing functionally graded microstructures and optimization of the processing technique to create a robust linkage between processing parameters and the desired microstructure. Reported in the literature, the conventional methods of ceramic processing such as screen printing have been used only for manufacturing compositionally graded cathodes. Moreover, existing techniques for producing functionally-graded electrodes require the deposition of multiple layers of material, each with different pore size that has been made using pore formers. Various physical and chemical processes have been used for preparation of porous electrodes; however, none of them has been utilized for processing of FGM cathodes. Besides, powder sintering routes such as slurry coating and screen printing require a relatively high sintering temperature for densification which usually causes undesired microstructures, because the three components require different firing temperatures [40]. Sol-gel [41-43] gel-casting [44] and screen printing which suffer from crack formation and require sintering at elevated temperatures. Tape casting, tape calendaring and screen printing are appropriate for small area cells and the quality will be reduced in large area cells [45-48]. Also, vapor deposition techniques require sophisticated apparatus and a controlled atmosphere which increases the cost of fabrication. Moreover, stoichiometric multi-component oxide films are

difficult to be produced using chemical vapor deposition (CVD) and electrochemical vapor deposition (EVD) methods because different precursors have different rate of vaporization [40].

Spray pyrolysis is one of the most cost effective techniques with simple apparatus for deposition of uniform thin films of large surface areas under atmospheric conditions. It is performed at a relatively low temperature and at a high deposition rate. It has the capability of controlling the shape, size, composition and phase homogeneity of the particles due to the easy control of parameters. The extremely large choice of precursors along with simple equipments for mass production of large areas have made spray pyrolysis an industry compatible manufacturing technique for synthesis of porous films with well-controlled microstructures. It has a great potential for producing functionally-graded electrodes that require the deposition of multiple layers of material, each with a different pore structure [49-51].

In this work, a novel ultrasonic spray pyrolysis is developed to study the effect of deposition spray deposition parameters on the microstructure and morphology of the LSM film. A gradient porous LSM cathode was processed for use in IT-SOFCs with the processing conditions optimized through varying the deposition parameters such as the type of the solvent, temperature, and solution flow rate.

CHAPTER 2

LITERATURE REVIEW

2.1 Fundamentals of Fuel Cells

Fuel cells currently being investigated are generally classified into five types, based on their difference in electrolyte material: polymer electrolyte fuel cells (PEFCs) or proton exchange membranes (PEM), alkaline (AFCs), phosphoric acid (PAFCs), direct methanol (DMFC), molten carbonate (MCFCs) and solid oxide fuel cells (SOFCs). The main sources of fuels used for feeding these fuel cells are pure hydrogen (AFC, PEFC, PAFC), diluted methanol (DMFC), and H_2- and CO-rich gas mixtures that result from reforming or partial oxidation of hydrocarbons (MCFC, SOFC). Among these types of fuel cells, proton-exchange membrane (PEM) and solid oxide fuel cells (SOFCs) with all solid components are currently the most attracting technologies for automotive and stationary applications due to the potential for higher power and energy densities [52]. Fig. 2.1 demonstrates the schematic of various types of fuel cells and their common components with different cell reactions and operating temperatures. The fundamental reaction in a fuel cell is:

$$2H_2 + O_2 \rightarrow 2H_2O \qquad\qquad (2.1)$$

The fuel cell membrane is mainly composed of the cathode, electrolyte and the anode. The task of the fuel cell membrane is to separate the oxygen and hydrogen gases such that it prevents a direct reaction between these two gases and the corresponding partial reactions, which is the oxidation of the hydrogen that is supplied from the fuel side (anode):

$$H_2 \rightarrow 2H + 2e^- \qquad\qquad (2.2)$$

and the reduction of oxygen that is supplied from the air side (cathode):

$$O_2 + 4e^- \rightarrow 2O^{2-} \qquad\qquad (2.3)$$

Then, the oxygen ions are transported from the air electrode (cathode) through a gas tight electrolyte. The electrons then move along an outer circuit to the cathode. When other fuels such as hydrocarbons are used, the fuel gas should be first reformed to hydrogen and carbon dioxide through direct reformation or via a shift reaction (intermediate generation of carbon monoxide) and then the pure hydrogen will be supplied to the fuel membrane [53].
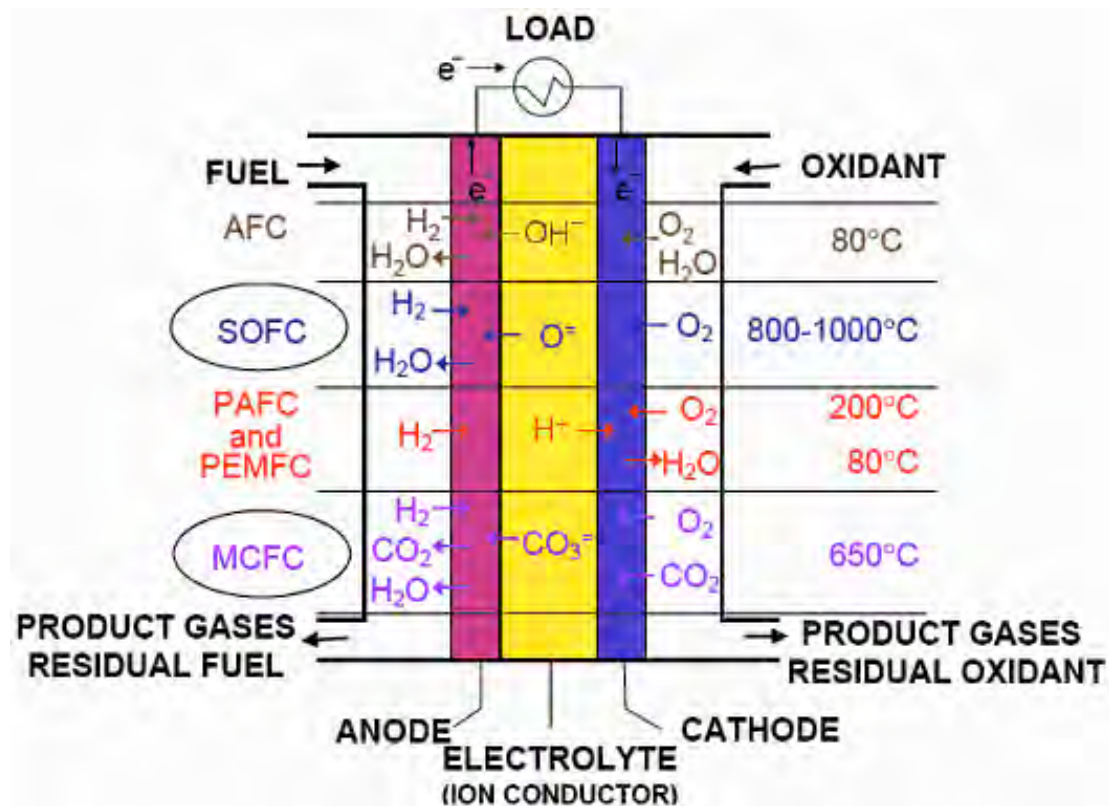
Figure 2.1. Schematic of various types of fuel cells with common components and different cell reactions and operating temperatures.

15

2.2 Solid Oxide Fuel Cells

Solid oxide fuel cells (SOFCs) are solid-state electrochemical devices that convert electrochemical energy directly to electrical energy with 45-50% electrical efficiency. SOFC cell components are constructed from ceramic materials which can tolerate operating temperature in the range of 800-1000. In fact, high operating temperatures facilitates utilizing the byproduct heat in a bottoming cycle (such as fuel reforming) for electric power generation which leads to a further improvement in the overall efficiency up to more than 80%. It also improves tolerance to impurities in the fuel. Accordingly, SOFCs have the capability of operating with both current fossil-based and future hydrogen-based fuels [2]. At high temperatures, however, expensive interconnect materials are required and degradation of SOFC components is hastened. These factors have driven researchers to find new ways to reduce the operating temperature of SOFCs.
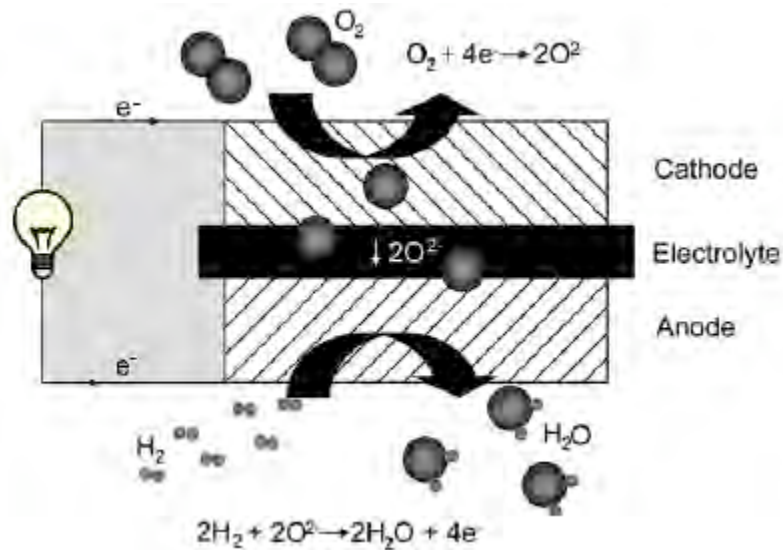

Fig. 2.2. Schematic of a SOFC.

At the present time SOFC technology is still in development to overcome challenges that are mainly dealing with design and low cost processing of functional components that can operate longer at low temperatures.
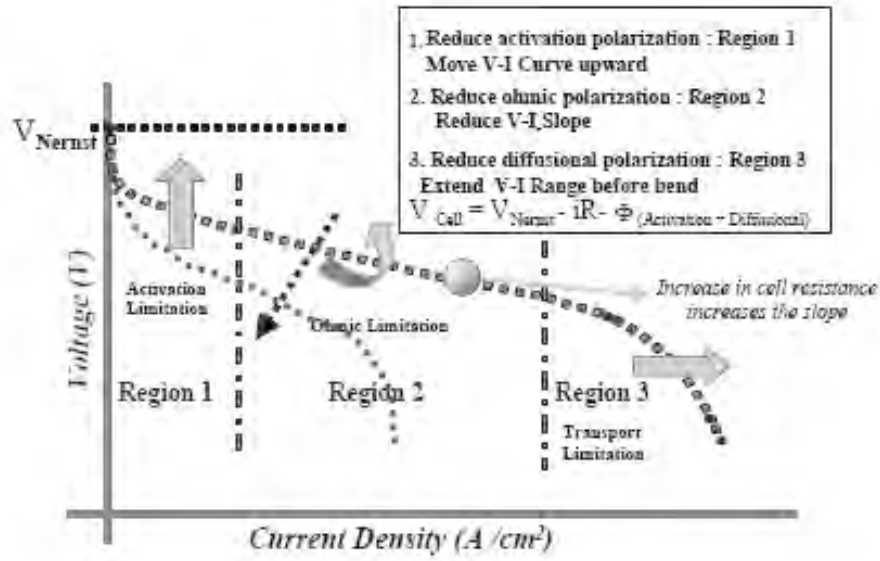
Fig. 2.3. Current–voltage characteristic of an electrochemical cell. Electrical performance losses are attributed to activation (Region 1), resistance (Region 2), and mass transport (Region 3). Cell electrical performance degradation is attributed to electrode deactivation, poisoning, and increase in cell resistance [54].

The thermodynamically maximum voltage obtainable for a given temperature (E^0) is calculated according to Eq. 2.4, in which (ΔG^0) is the Gibbs free energy difference between fuel cell products and reactants and $n = 2$ is the number of equivalent electrons per mole reacted:

$$E^0 = -\Delta G^0/nF \tag{2.4}$$

The Nernst voltage can be calculated for a H_2/O_2 fuel cell by:

$$E = E^0 + RT/2F \; (ln(P_{H2}P_{O2}^{0.5}/P_{H2O})) \tag{2.5}$$

The operational fuel cell voltage which is the cell voltage under a close circuit condition, E_{op} is always less than the open circuit voltage, E which is the ideal Nernst voltage calculated from thermodynamic principles according to Eq. (2.6).

$$\eta = E - E_{op} \tag{2.6}$$

The difference between the cell and reversible voltage is called polarization or overpotential and it is caused by three major phenomena. H_Ω is the overpotential caused by electronic and ionic ohmic resistances from current flowing through the electrodes or the electrolyte whereas it can be further divided into the charge transfer (also called activation) polarization, η_{ct}, across an electrode. Mass transfer or concentration polarization, η_{mt}, is the voltage loss caused by reduced fuel and oxidant concentrations when the rate of transferring reactants to or products away from the reaction sites is slower than the rate of the charge transfer processes:

$$\eta = \eta_{electrolyte} + \eta_a + \eta_c \qquad (2.7)$$

$$\eta = \eta_\Omega + (\eta_{ct,a} + \eta_{mt,a}) + (\eta_{ct,c} + \eta_{mt,c}) \qquad (2.8)$$

The electrical output of an electrochemical cell is represented by a "Current-Voltage" relationship as shown in Fig. 2.3 At lower current densities, electrical performance loss in the cell is attributed to activation or charge transfer process limitations (Region 1) whereas at higher current densities, resistive (Region 2) and mass transport (Region 3) processes limit the overall performance [32, 54].

SOFC Stack Designs

A SOFC single cell stack can be designed in four configurations: the planar design, the tubular design, the segmented-cell-in-series design, and the monolithic design. Planar cell configuration is a single cell with common plate shapes rectangular or circular configured as flat plates which are connected in electrical series. The cell is mechanically supported by either each of the cell components or interconnects. The cell with tubular design is composed of the cathode component inside (cathode supported) and electrolyte and anode layers on the outside of the tube. In segmented-cell-in-series design, the

segmented cells are connected in electrical and gas flow series. The cells are either arranged as a thin banded structure on a porous support or fitted one into the other to form a tubular self-supporting of a bundle of single cell tubes. Monolithic design consists of cell components formed into a corrugated structure of either gas co-flow or crossflow configurations. Currently, tubular and planar designs are the most common designs while the monolithic and segmented cell-in-series designs are less developed. Fig. 2.4 depicts the most popular tubular and planar designs. One drawback of tubular design is their high internal ohmic loss compared to planar design which is associated to relatively long in-plane path for electrons to travel along the electrodes to and from the cell interconnects. In planar design, main problems are typically related to sealing the stacks to prevent fuel and oxidant gases mixing and the thermal mismatch between ceramic components, which has led to cracking during thermal cycling [52].
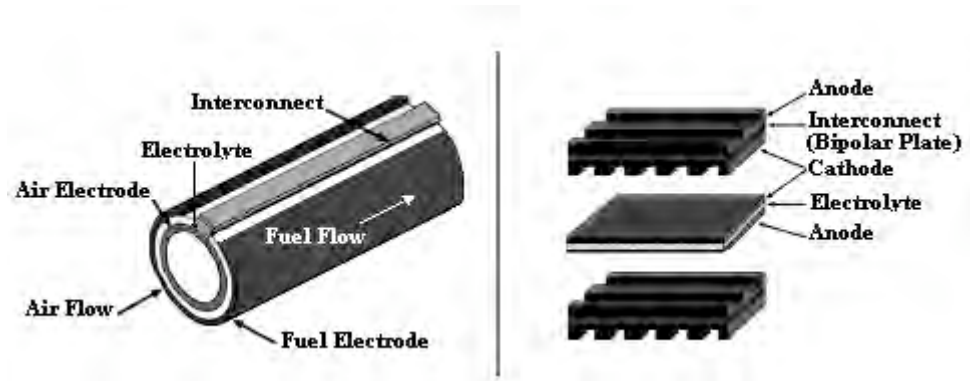

Fig. 2.4. Solid oxide fuel cell configurations. Left: Tubular design and right: Planar design.

SOFC Single Cell Configurations

The desire for achieving high power density requires the individual layers of the SOFC cell to be made as thin as possible. However, all of the cell components could not be very thin at the same time, since they may crack or break without mechanical support.

To overcome this problem, one of the cell components is usually chosen to be thick enough to be able to mechanically support the cell. Illustrated in Fig. 2.5, there are five general ways of cell supporting designs in planar design in which three architectures of electrolyte supported, anode supported and cathode supported cells are mostly in use [6, 52]. Each design has some advantages and disadvantages that are summarized in Table 2.1.
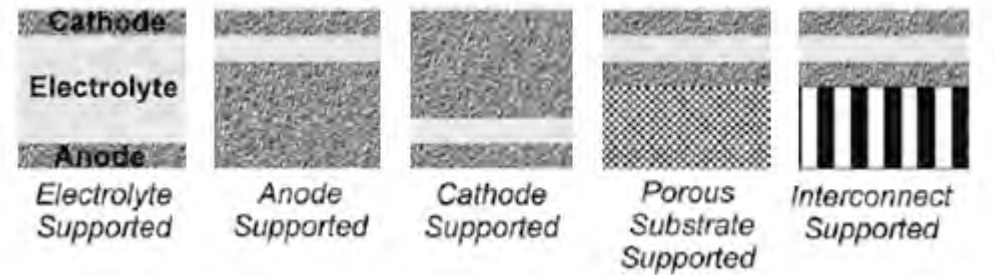
Fig. 2.5. Illustration of the different types of cell support architectures for SOFCs [6]

Table 2.1. Main features of single cell configurations [55]

Cell configuration	Advantages	Disadvantages
Self-supporting		
Electrolyte-supported	Relatively strong structural support dense electrolyte; Less susceptible to failure due to anode re-oxidation and cathode reduction	Higher resistance due to low electrolyte conductivity; Higher operating temperatures required to minimize electrolyte ohmic losses
Anode-supported	Highly conductive anode; Lower operating temperature via use of thin electrolytes	Potential anode re-oxidation; Mass transport limitation due to thick anodes
Cathode-supported	No oxidation issues but potential cathode reduction; Lower operating temperature via use of thin electrolyte	Lower conductivity; Mass transport limitation due to thick cathodes
External-supported		
Interconnect-supported	Thin cell components for lower operating temperature; Strong structures from metallic interconnects	Interconnect oxidation; Flow field design limitation due to cell support requirement
Porous substrate	Thin cell components for lower operating temperature; Potential for use of non-cell material for support to improve properties	

2.2.1 Materials for SOFCs Components

The requirements for choosing appropriate materials for SOFC cell components is determined by functions of each component in the cell. Among perovskite oxides, $La_xSr_{1-x}MnO_{3\pm\delta}$ (LSM) is the best candidate commonly used as the cathode.

1. Cathode

In SOFCs, cathode is the component at which the electrochemical reduction of the oxygen gas occurs. The cathode material and microstructure should be designed such that it provides sufficient porosity to enhance oxygen transport and it also demonstrates sufficient catalytic activity for oxygen reduction, stability at fabrication and operating temperatures and good electronic conductivity at the operating conditions. One way to incorporate all above requirements into the cathode microstructure is to design functionally graded cathode which could exhibit both electronic and ionic conduction in compositionally graded MIECs and maintain mechanical, electrical and mass transport properties at optimized level in porosity graded structures.

Main concerns for materials being chosen as the SOFC cathode are associated with having high electrical conductivity and thermal expansion compatibility with the electrolyte material. The most common cathode materials for oxygen reduction are perovskite oxides doped with lower valence cations which show intrinsic p-type conductivity due to cation vacancy formation at high temperatures in oxidizing atmospheres. So far, strontium-doped lanthanum manganite (LSM) has been extensively used as the cathode material for SOFCs with thermal properties matching YSZ electrolyte. The LSM cathode demonstrates the highest electrical conductivity at high temperatures since the increases the content of Mn^{4+} in place of Mn^{3+} according to

$$SrO \xrightarrow{\text{LaMnO3}} La_{1-x} Sr_x Mn^{3+}{}_{1-x} Mn^{4+}{}_x O_3 \qquad (2.9)$$

2. Electrolyte

SOFCs electrolytes should provide a good pass for oxygen ions transfer from the cathode to the anode side of the cell. Therefore, the main characteristic of the electrolyte is to be ionically conductive and electronically insulative. The thickness of the electrolyte is a critical factor that affects ionic conductivity as well as the ohmic polarization. Practically, electrolyte supported geometries show high ohmic resistance at lower temperatures of operation, even if they are designed to show high ionic transport properties. Yttria stabilized zirconia (YSZ) is the most widely used electrolyte for SOFCs. Doping lower oxidation state cations such as Y^{3+} in zirconia (ZrO_2) based materials will generate oxygen vacancies, so increasing the oxide ion conductivity [6].

3. Anode

The anode must be porous to allow fuel gas in while it acts as a catalyst for fuel oxidation and must show electronic and ionic conductivity as well. Using two-phase cermets (ceramic-metal composites) such as YSZ or cerium gadolinium oxide (CGO) ceramic electrolytes as the ionic conductors in combination with nickel would provide all three properties required for functionality of the anode.

Functionally Graded Materials (FGMs)

Functionally graded materials (FGMs) have been developed for SOFCs as a method to enhance overall performance by improving functionality of the individual layers. Grading can be classified in three ways: (1) composition grading (volumetric ratio

of electronic conducting particles to ionic conducting particles), (2) particle size grading, and (3) porosity grading. In either ways, the goal is to enhance the electrochemical reactivity and increase the electronic/ ionic conductivity of the electrode, to minimize the mass transport resistance to gas mixtures and thus concentration polarization inside the porous electrode and to increase mechanical stability by, for instance, avoiding sharp discontinuities in thermal expansion coefficients, which could result in delamination during thermal cycling [33, 36, 56].

The relative effect of composition and porosity gradients in a porous composite electrode is then theoretically studied to better understand the behavior of a graded electrode. It has shown that a fine microstructure is effective in lowering the activation polarization, assuming that porosity is high enough to prevent concentration polarization (related to the diffusion process of gases through the gas-filled pores of the electrode to reach reaction sites). The reported results clearly indicate that grading composition is helpful to improve ionic transport through the electrode and, thus, electrochemical performances for operating temperatures lower than 800 °C.

2.2.2 Fabrication Techniques for SOFCs Cathodes

SOFC components are fabricated using a wide range of methods. However, two general approaches are mainly applied depending on the type of processing technique, namely, particulate approach and deposition approach. Using ceramic powders in particulate approach, the cell component is fabricated through consolidation and sintering of the ceramic powder. On the other hand, deposition approach involves formation of cell components on a substrate via a physical or chemical deposition process [55].

The performances of electrodes are dramatically influenced by the processing conditions. The most commonly used approaches for electrode fabrication are slurry coating [57], slurry painting, spin coating [58] screen printing [59]. Thin film deposition techniques such as physical and chemical deposition processes have the potential of providing control over processing parameters and therefore there is an opportunity to utilize these techniques over the conventional methods to optimize the microstructure of the SOFC components.

2.2.2.1 Thin Film Deposition Techniques

Thin film deposition techniques have been divided into two major processes: physical deposition and chemical deposition processes [60]. As shown in Fig. 2.6, the physical methods include physical vapor deposition (PVD), laser ablation, molecular beam epitaxy, and sputtering. The chemical methods comprise gas phase deposition methods and solution techniques. The gas phase methods include chemical vapor deposition (CVD) and atomic layer epitaxy (ALE), while in spray pyrolysis, sol-gel, spin coating and dip coating methods deposition of precursor solutions is employed.

Spray Pyrolysis

This coating technique was the predecessor of the chemical vapor deposition (CVD) techniques. The coating is applied at elevated temperatures by spraying droplets of liquid precursors onto hot substrates. The major advantages of spray pyrolysis are that the coatings are more durable than vacuum deposited coatings, the variety of precursors could be used, and the process can be employed at lower cost than CVD or vacuum

deposition. The disadvantage is that the coatings are not uniform in thickness. CVD consists of vaporizing the precursors and directing the resultant gases onto a hot substrate.
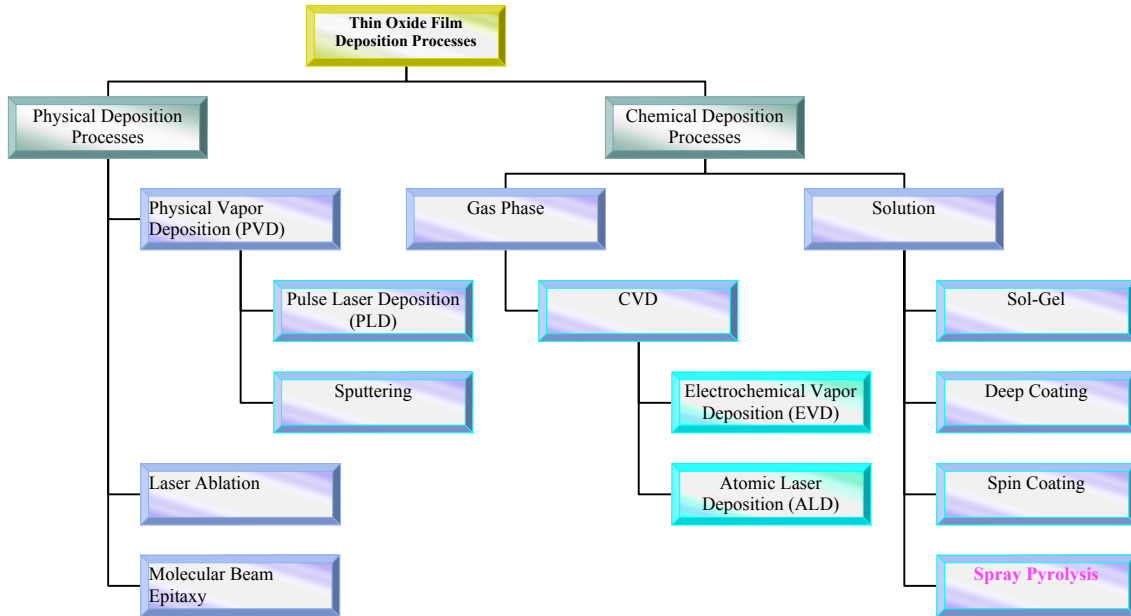

Fig. 2.6. Classification of thin film deposition techniques.

Spray pyrolysis is a versatile processing technique for preparation of dense and porous single and multi-layered films, ceramic coatings and powders of various materials and morphologies. [61] Classification of different spray processes could be made based on the type of energy source for the precursor reaction such as spray pyrolysis in a tubular reactor (SP), vapor flame reactor (VFSP), the emulsion combustion method (ECM) and flame spray pyrolysis (FSP) [62] or the method of atomizing the precursor, namely air pressurized, electrostatic and ultrasonic spray pyrolysis [63]. In the case that the energy source for precursor reaction is an external energy supply and not from the spray itself, (as in SP and VFSP), method is less sensitive to the choice of precursors and solvent.

Different types of solvents are used in spray pyrolysis depending on the type and solubility of the precursors and economic aspects. Nitrates, chlorides and acetates are typically chosen as the metal-oxide precursors that can be dissolved in aqueous and alcoholic solvents [62].

Advantages of Spray Pyrolysis

In comparison with other thin film deposition methods, spray pyrolysis has many advantages including: open-atmosphere process, open reaction chamber, easy access to observe the deposition process and adjustment during the experiment. It has also the multi-layer fabrication capability which is very attractive for making functionally graded films. The composition of the film can be adjusted by changing the precursor solutions. Spray pyrolysis is of great practical interest in processing dense and porous films for SOFC electrolyte and electrodes, by optimizing the deposition variables such as: deposition temperature, substrate temperature, precursor composition and concentration, solvent composition, solution flow rate, carrier gas ratio and flow rate, etc. Films can be also obtained on large surfaces at temperatures ~ 500 °C. One of the major advantages of spray pyrolysis over the vapor-phase routes is the possibility of producing multicomponent particles with exact desirable stoichiometry in the final product. Depending on the substrate temperature, precursor type, and the nozzle-to-substrate distance the droplets can evaporate or decompose completely before reaching the substrate, resulting in a process resembling to CVD (Fig. 2.7), or the liquid is deposited without evaporation. Burning a flammable precursor may also result in forming a particulate spray or to obtain higher deposition temperatures.
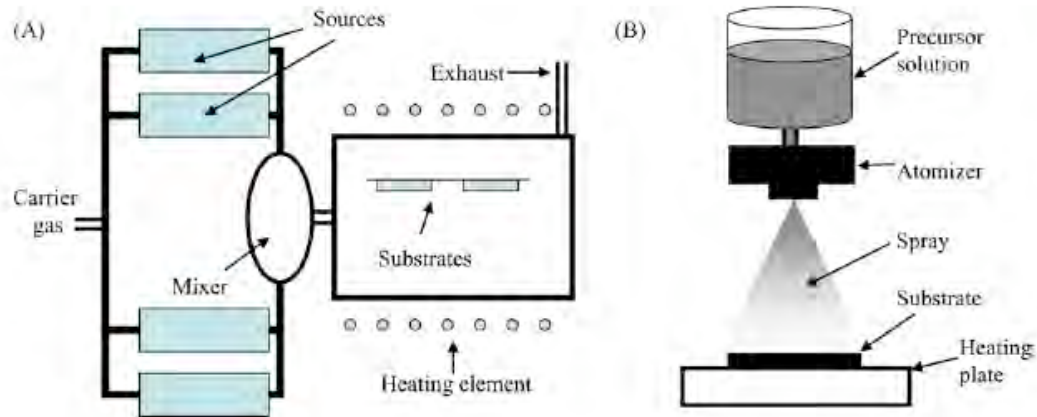
Fig. 2.7. (a) Schematic representation of a generic CVD reactor; (b) Schematic representation of a generic spray process.

There are too many processes that occur either sequentially or simultaneously during film formation by spray pyrolysis for these to be modeled in a straightforward manner. These include precursor solution atomization, droplet transport and evaporation, spreading on the substrate, drying and decomposition of the precursor salt. Understanding these processes will help to improve film quality. Thin film deposition using spray pyrolysis can be divided into three main steps: atomization of the precursor solution, transportation of the resultant aerosol and decomposition of the precursor on the substrate. However, four types of processes that may occur during deposition are shown in Fig. 2.8. In process 1, the droplet splashes on the substrate, vaporizes, and leaves a dry precipitate in which decomposition occurs. In process 2, the solvent evaporates before the droplet reaches the surface and the precipitate impinges upon the surface where decomposition occurs.
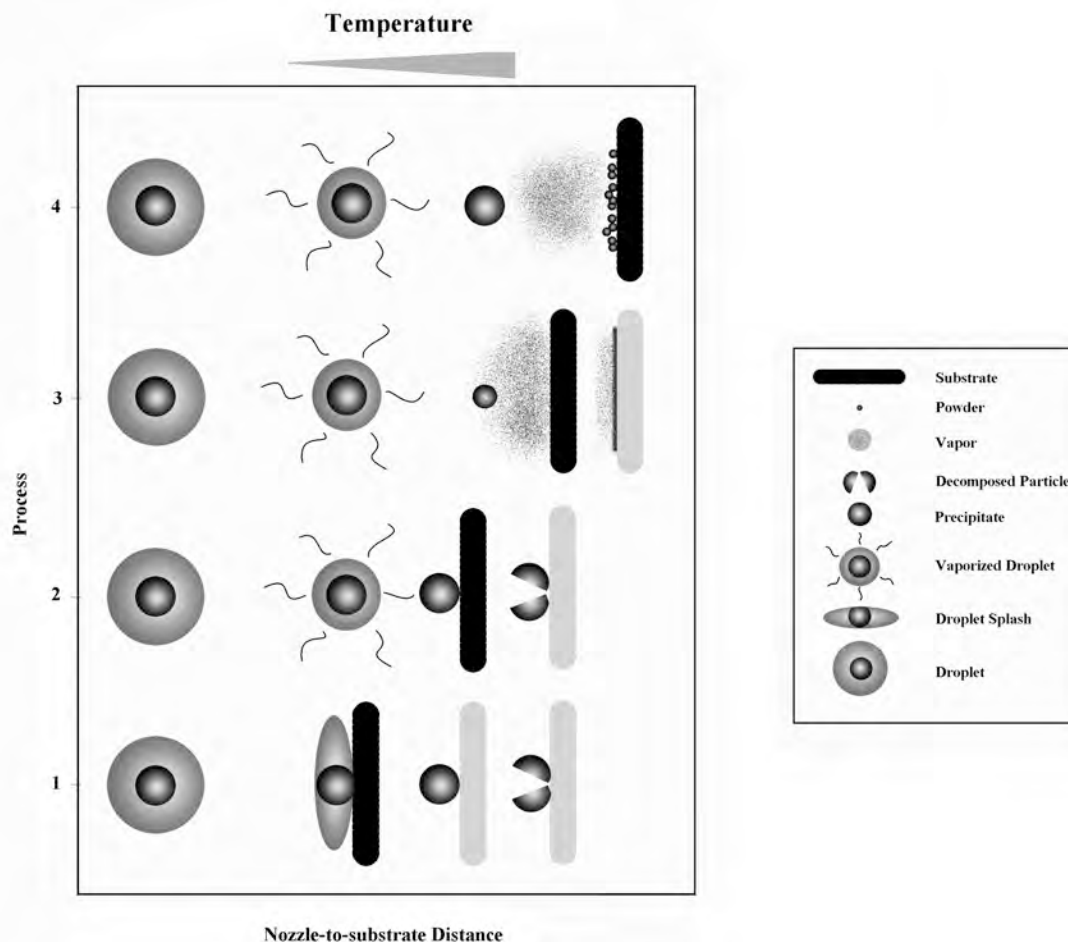
Fig. 2.8. Schematic depicting different deposition processes that occur as the nozzle-to-substrate distance and deposition temperature change.

In process 3, the solvent vaporizes as the droplet approaches the substrate, then the solid melts and vaporizes (or sublimes) and the vapor diffuses to the substrate to undergo a heterogeneous reaction there. This is true CVD. In process 4, at the highest temperatures, the metallic compound vaporizes before it reaches the substrate and the chemical reaction takes place in the vapor phase [64].

The type of spray pyrolysis is usually attributed to the type of the atomizer that is used in the system. Also, the droplet size of the aerosol is generally dependent on the atomization method, which in turn determines the film quality. There are three major types of atomizers: air blast, electrostatic, and the ultrasonic. The spray pyrolysis

technique using the electrostatic atomizer is called Electrostatic Spray Deposition (ESD), the technique using the air blast atomizer is named Pressurized Spray Deposition (PSD), and the technique using Ultrasonic atomizer is generally recognized as the ultrasonic or normal Spray Pyrolysis (SP).

Table 2.2. Characteristics of atomizers commonly used in spray pyrolysis [65]

Atomizer	Droplet size (µm)	Atomization rate (cm^3/min)
Pressure	10-100	3-no limit
Nebulizer	0.1-2	0.5-5
Ultrasonic	1-100	<2
Electrostatic	0.1-10	

Ultrasonic atomization relies on an electromechanical device that vibrates at a very high frequency. Only low-viscosity Newtonian fluids could be atomized by passing over the vibrating surface and the vibration causes the fluid to break into droplets. Fig.1 shows an example of ultrasonic atomization technology.
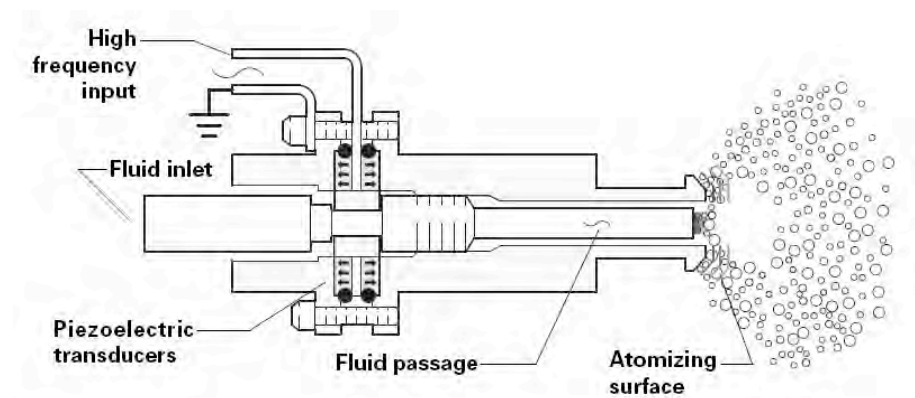
Fig. 2.9. Schematic of an ultrasonic atomizer.

The type of pray technique used in this study is an ultrasonic spray pyrolysis in a tubular reactor. In this method, the precursor solution is atomized into a hot-wall reactor and each atomized droplet serves as a microreactor which is delivered by carrier gases to the reaction site and undergoes solvent evaporation, decomposition and precipitation to form the final product film or particle. The ratio of deposition temperature to solvent boiling point is found to be the most important processing parameter that determines whether a crack free homogeneous and coherent film is obtained [63].

CHAPTER 3

EXPERIMENTAL PROCEDURES

In this chapter, the experimental procedures for developing the novel spray pyrolysis system and its implementation in processing of multi-layered LSM cathode based on optimization of processing parameters are explained in detail. Through several set of experiments, the range of initial spray conditions such as precursor and solvent type, solution concentration, nozzle-to-substrate distance, carrier gas flow rate, deposition temperature and solution flow rate, over which the LSM film could be reproducibly deposited in the stoichiometric ratios on YSZ substrate was determined. Based on the results of this stage, some of the critical parameters were set to be fixed at their required values, and the effects of main deposition parameters were determined in the second set of spray experiments. Using data from the second set of experiment, conditions for processing a multi-layered gradient porous LSM on the YSZ substrate were identified. The gradient porous LSM cathode was successfully deposited on YSZ. The film crystalline phases, composition, and microstructure were characterized by XRD, EDS and SEM. BET surface analysis was applied to obtain the pore size distribution. Electrical conductivity measurement was also conducted to understand the effect of gradient porosity structure on the electrical conductivity of the film at operating temperatures.

3.1 Development of a Novel Spray Pyrolysis System

3.1.1 Ultrasonic Spray Pyrolysis Setup

Shown in Fig. 3.1 and 3.2, show the schematic and the photograph of the novel horizontal spray pyrolysis setup that has been developed in our laboratory. Similar to other spray systems it consists mainly of the spraying unit, the liquid feeding unit, and the temperature control unit. The type of spray pyrolysis method used in this work is a spray pyrolysis in a tubular reactor. The solution is prepared by dissolving the stoichiometric ratios of the desired precursors into solvent using a magnetic stirring. The solvent is pumped (Stroke pump) to a 100 kHz ultrasonic atomizer (Lechler Inc.) toward the heated substrate held inside a tubular quartz reactor (5 cm in i.d. and 30 cm in length). The substrate was mounted on the graphite sample holder and heated by quartz heating bulbs located on top and below the tube. The substrate temperature was monitored by a type K thermocouple connected to the temperature controller monitor. Once the temperature controller showed the desired temperature, the solution was pumped into the atomizer and the atomized droplets of the precursor were sprayed and transported toward the substrate to the reaction chamber using nitrogen (N_2) and oxygen (O_2) as the carrier gases. Upon reaching the hot surface of the YSZ substrate, the aerosol droplets were decomposed and converted to very small particles of the oxide compounds. The average spray time for all samples was around 30-45 min depending on the spray conditions.

The novelty of our spray pyrolysis system relies on modifying the traditional commonly used vertical system to a horizontal system in which the deposition process takes place similar to liquid delivery chemical vapor deposition (LD-CVD) in a way that it could take the advantage of both techniques. One aspect is related to the use of quartz

lamps as the heating source and heating the YSZ substrate from both top and bottom of the substrate. Since YSZ is thermally insulative and has low thermal conductivity-it is usually used as a thermal barrier coatings- the pellet has always lower temperature on its surface than what is usually measured at the bottom and where it is directly in contact with the heating element. Therefore, this difference may result inaccuracy in reporting the temperature required for the reaction to take place as well as cracking the substrate as we observed in our preliminary results. Also, development of organometalic precursors for fabrication of thin films of oxide cathodes in subsequent results showed to be promising in controlling the particle/pore size and achieving the desired morphology and microstructure.
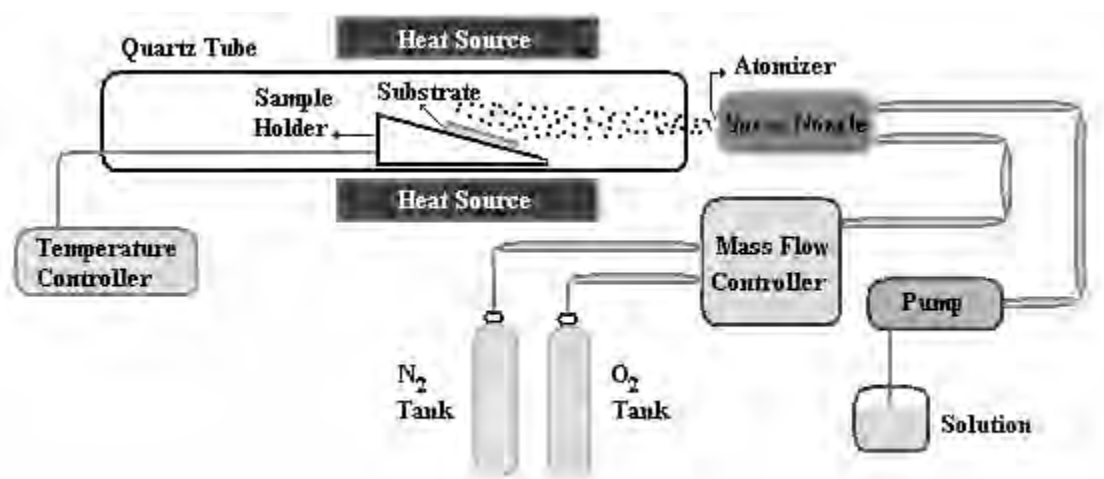
Fig. 3.1. (a) Schematic of the spray pyrolysis setup.
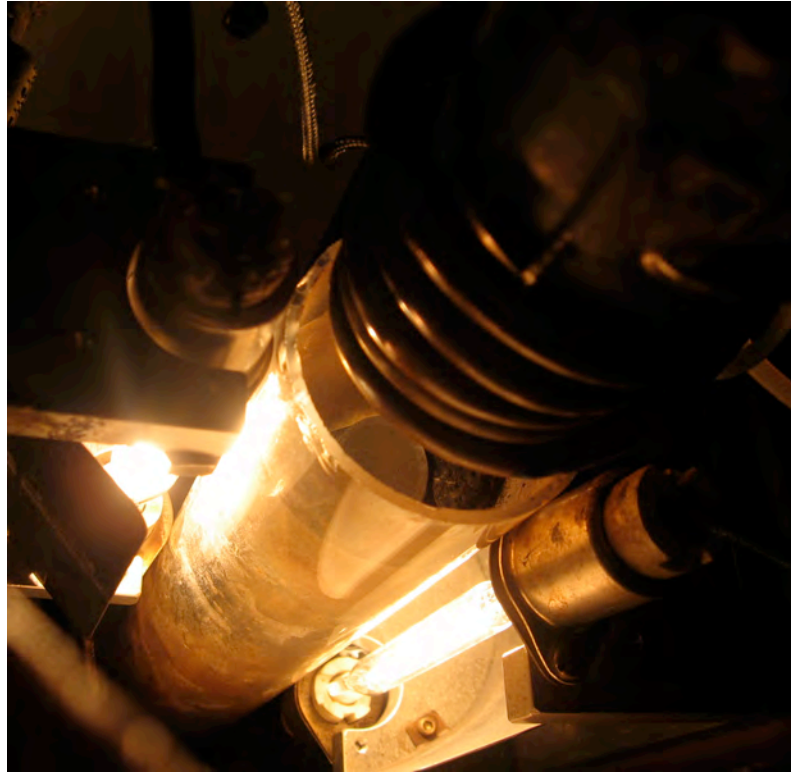
Fig. 3.2. Photograph of the spray pyrolysis setup.

3.2 Deposition of LSM cathode by Spray Pyrolysis

3.2.1. Preparation of the YSZ electrolyte substrates

YSZ electrolyte substrates were prepared from pressing 8 mol% yittria stabilized zirconia (TZ8Y) powders from Tosoh Co. into pellets of 2.5 cm in diameter and thickness of about 1 mm by a hydrostatic press (Buehler Ltd). To make a dense electrolyte substrate, the pellets were sintered at the heating rate of 4 ºC/min up to 1400 ºC at air atmosphere, held for nearly 1 h and then cooled down to room temperature with the same cooling rate of 4 ºC/min.

3.2.3. Effect of Precursors and solution type

The choice of a salt and the solvent is the first important task before parameter optimization. The optimal spray parameters usually differ considerably for each type of salt and are strongly dependent on the physical properties of the solvent. In the first stage, the experiment was conducted to find the appropriate precursor materials and processing parameters to produce a well-controlled porous LSM microstructure on YSZ substrate. For this purpose, two starting systems were examined; the starting aqueous solution was made by dissolving stoichiometric ratios of metal acetates precursors of lanthanum, strontium and manganese in deionized water and was sprayed to the YSZ substrate at 480 ºC with the oxygen to nitrogen gas flow rate of 80/400 ml/min. Also, a pure organic solution containing metal-organic precursors was prepared and sprayed on the YSZ at the same temperature and solution flow rate as for aqueous solution. Using metal β-diketonates, the volatile metal-organic precursors as what is used in CVD, metal 2,2,6,6-tetramethyl-3,5 heptanedionates-TMHD from Strem Co. (also known as La(TMHD)$_3$, Sr(TMHD)$_2$, Mn(TMHD)$_3$) were dissolved as the metal-organic precursors of La, Sr, and Mn in appropriate ratio into dimethylglycol or ethylene glycol dimethyl ether with molecular formula of $CH_3OCH_2CH_2OCH_3$ to achieve reproducible stoichiometric ratio of the film composition La:Sr:Mn = 0.75:0.25:1. The nozzle to substrate distance was kept constant at 6.4 cm in all stages of the experiment. A heat treatment was also conducted on both samples in an electric furnace at 750 ºC for 4 hours and finally cooling to room temperature in about 5 hours.

3.2.4. Adjusting the Deposition Parameters

To determine the effect of spray parameters on the film quality, morphology and microstructure, temperature and solution flow rate on the morphology and the microstructure of the LSM cathode film, the solutions were deposited on the YSZ substrate at four different temperatures of 520, 540, 560 and 580 ºC and at three different solution flow rates of 0.73, 1.13, 1.58 ml/min. Based on the results of this part, deposition conditions were adjusted for spraying metal-organic precursors and organic solvents similar to those used in liquid delivery CVD. In this stage, the same metal-organic precursors were weighted to the stoichiometric ratio and dissolved in ethylene glycol dimethyl ether as organic solvent.

3.2.3. Deposition of the gradient porous LSM cathode

Finally, based on the results of previous stage, spray pyrolysis in multiple speed-temperature spray steps was applied to deposit a gradient porous LSM cathode layer on the YSZ substrate. In order to create a nanocrystalline thin layer on the surface of the substrate and have surface reactions completed, first, a dilute solution with the same stoichiometric composition was prepared containing lower concentration of metal-organic precursors in 100 ml of dimethoxyethane as the solvent and was sprayed at 520 ºC. In the next stage, 4× concentrated solutions were made of the same metal-organic precursors in 50 ml dimethoxyethane to be used in producing gradient porous layers via different temperature- speed sprays on the first layer. Oxygen/Nitrogen carrier gas flow was kept constant at 80/800 ml/min.

3.4 Characterization Techniques

3.4.1 Adhesion Test

Before doing any characterization on the as-prepared and heat treated films, adhesion strength between the films and the substrates were evaluated by applying the Scotch tape test on the deposited films. Generally, adhesion strength is considered to be "good" if the film adheres to the substrate and it doesn't peel off the substrate.

3.4.2 Scanning Electron Microscope

A Hitachi S-800 and a LEO 1530 Scanning Electron Microscopes (SEM) were used to characterize the particle morphology, pore microstructure surface and cross sectional structure of the sample in terms of three-dimensional features, pore size and its distribution, and microstructure changes with changing deposition parameters.

3.4.2.2 Energy Dispersive X-Ray Spectroscopy

Energy Dispersive X-Ray Spectroscopy was used for the elemental analysis and chemical characterization of a sample. Compositional homogeneity of the film was also analyzed via recording the composition maps.

3.4.2.3 X-ray Diffraction

X-ray diffraction has been used to identify the crystalline phases of the materials based on the Bragg's law. As shown in Fig. 3.3, condition at which diffraction occurs in a crystalline material satisfying the Bragg's law is described as:

$$n\lambda = 2d \sin\theta \qquad\qquad (3.1)$$

where λ is the wave length of the X-ray beam, d is the spacing between the planes in the atomic lattice, θ is the angel between the incident ray and the scattering planes, and n is

an integer. Waves that satisfy this condition interfere constructively and result in a reflected wave of significant intensity.
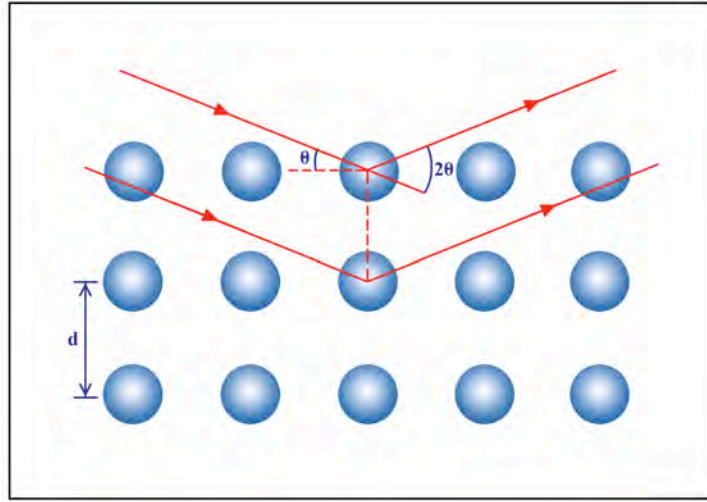

Fig. 3.3. Schematic of X-ray diffraction.

Crystalline phases of as-prepared and heat treated films were characterized by X-ray diffraction using Philips X'Pert MRD Diffractometer, performed at 40 kV and 45 mA using Cu-Kα monochromatic radiation. Also, the effect of heat treatment on phase crystallinity and phase stability of the multi-layer LSM film was studied by performing an in situ high temperature X-ray diffraction measurement on the as-prepared multi-layer LSM by a PANalytical X'pert Pro MPD diffractometer and an Anton-Paar HTK1200 high-temperature furnace. The peaks were recorded in the heating regime of room temperature to 900 ºC with heating rate of 50 ºC min^{-1} and 100 ◦C temperature intervals between 300 to 900, followed by a 4 hour heat treatment at 700 ºC. The XRD peaks were compared with JCPDS cards for phase identification.

Using Scherrer formula mean crystallite size of the LSM film (D) was obtained from the following equation:

$D = 0.9\lambda / \beta \cos \theta$ (3.2)

where $\lambda = 1.541$, θ is the diffraction peak angle, and β denotes the full width at half maximum (FWHM) of the corresponding diffraction peak.

3.4.2.3 Surface Area and Pore Size Distribution Analysis

The surface area and the pore volume of the graded porous LSM film were determined by Bruanuer-Emmett-Teller (BET) method using a SA 3100 surface area and pore size analyzer, based on adsorption of monolayer of gas molecules on the solid surface. N_2 adsorption measurements on samples degassed for 4 h at 300°C. Using adsorption and desorption isotherms the amount of gas molecules adsorbed on the surface can be determined.

The BET equation is expressed by Equation (3.3):

$$\frac{1}{V_A\left[\left(P_0/P_S\right)-1\right]} = \frac{C-1}{V_M C}\left(\frac{P_S}{P_0}\right) + \frac{1}{V_M C} \qquad (3.3)$$

where V_A is the volume of gas adsorbed and P_S and P_0 are the equilibrium and saturation pressure of adsorbed gas at the temperature of adsorption, , V_M is the volume of the monolayer adsorbed, and C is the BET constant, Equation (3-2) can be plotted as a straight line with $1/(V_A((P_0/P_S)-1))$ versus the relative pressure P_S/P_0 to give the BET plot. Pore size distribution was determined using

 3.4.2.4. Electrical Conductivity Measurement

Fig. 3.4 shows the schematic of a four point probe setup consist of four equally spaced tips that are made of high temperature resistant material. The four tips are part of an auto-mechanical stage that moves up and down during the measurement to make sufficient contact between the tips and the film. The temperature dependent electrical conductivity of the LSM cathode films was measured using a four-point probe setup combined with a micro-heater for heating the sample up to its operating temperature i.e., 700 °C. Measurement was performed in a temperature range from 250 to 700 °C, with the heating and cooling rate of 10 C/min in the ambient atmosphere. For a material with a fixed known thickness t, electrical conductivity of the sheet σ (sheet resistivity) can be measured through four-point measurement method. In this method, a fixed DC current I (20 mA)is forced into material through two ports; then, the DC voltage V is measured at the other two ports. The setup consists of four equally spaced high temperature tips. The sheet resistivity of the thin film is then measured based on the following equation:
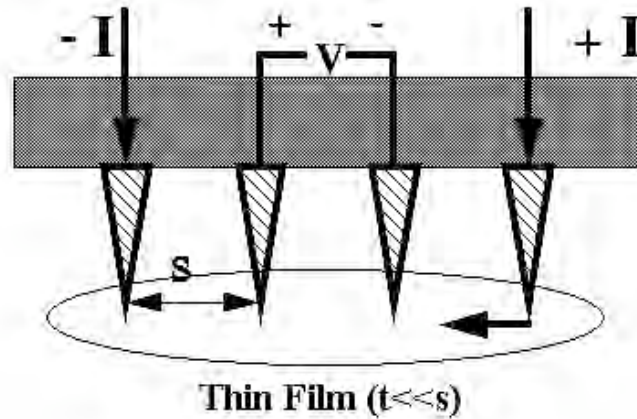
$$1/\rho = \sigma = (I/V)\ ln2/\pi t \qquad\qquad (3.6)$$

Fig. 3.4. Schematic of four point probe setup.

CHAPTER 4

RESULTS AND DISCUSSION

4.1. Effect of precursor materials and the solvent on the microstructure

Shown in Fig. 4.1 are some typical SEM images of the LSM thin films made from different precursors and solvents based on the specifications listed below. The sample made of the aqueous solution shows cracks throughout the surface. In fact, endothermic vaporization of water caused the surface temperature of this sample to be much lower than the heated surface of the YSZ. As a consequence of the temperature gradient, the resulting stress and strain distribution in the pressed YSZ pellets cause immature cracks and final failure (Fig. 4.1.a).

Aqueous solution:
Precursor: 110.6mg Lanthanum acetate, 30mg Strontium acetate, 86mg Manganese acetate,
Solvent: 25ml Methanol and 10ml water
Temperature: 480 °C
Oxygen/Nitrogen flow rate (m/min): 80/800
Solution flow rate: 0.73 (ml/min)

Organic solution:
Precursor: 80.3mg Tris Lanthanum, 22.7mg Bis Strontium, 100.7mg Tris Manganese,
Solvent: 50ml, Ethylene glycol dimethyl ether
Temperature: 480 °C
Oxygen/Nitrogen flow rate (m/min): 80/800
Solution flow rate: 0.73 (ml/min)

Moreover, layers of LSM on YSZ processed in water solvent show compositions that are not always very homogenous throughout the sample. According to Fig. 4.1.b,

microcracks formation was observed in aqueous solution after heat treatment which could also be attributed to fast cooling of the sample. As the cross sections in Fig. 4.1.c and d show, there are more pores and channels in the aqueous sample after heat treatment.

Crystalline phase analysis of the samples fabricated in stage A (Table 4.1) before and after heat treatment is shown in Fig. 4.2.a and b. The peaks indicate cubic YSZ substrate (JCPDS No. 01-089-6688) and rhombohedral phase of LSM (JCPDS No. 01-089-8097) before and after heat treatment. The comparatively sharp peaks apparent in the XRD patterns of as-prepared LSM confirm formation of non-amorphous film on YSZ. Also, sharp peaks of crystal phases imply increase of crystallinity after additional heat treatment. In addition, the results of this stage indicate that the solvent type contributes to the quality and morphology of the deposited film.
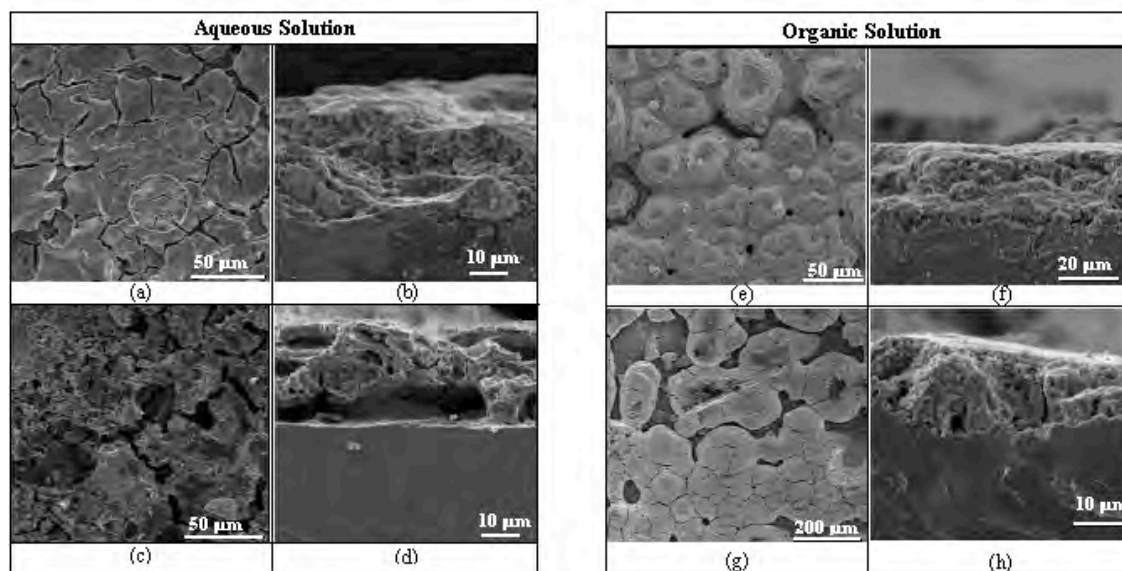
Fig. 4.1. SEM micrographs and cross sections of the LSM film made of aqueous (left) and organic (right) solutions; (a), (b), (e) and (f): before heat treatment; (c), (d), (g) and (h): after heat treatment.

However, in organic route, YSZ can act as an oxidizing catalyst helping the pyrolysis of metal-organic precursors and organic solvent. Here, spray pyrolysis of organo-metallic compounds is a combustion reaction in which the combusting droplets undergo an exothermic reaction and burst to form smaller and more stable oxide particles; as a result, due to the lower temperature difference between sprayed cathode and the heated YSZ surface no cracking occurred in YSZ substrate as it is shown in Fig. 4.1.c and d. Examination of the cross sections in Fig. 4.1.e and f reveals that the microstructure through the thickness did not show a lot of changes before and after heat treatment. Chemical analysis of the aqueous sample with EDS showed that the composition is not homogeneous throughout the film; however, it slightly improved after the heat treatment. Improvement is correspondent to the fact that the composition is close to the stoichiometry. In organic sample the lower amounts of Mn compared to the solution composition was observed in the film. This could be attributed to the volatility of the Mn precursor that in some cases does not result in deposition. Overall, both samples show slightly a porous microstructure which could be related to the very low temperature of deposition. It appears that the type of solvent has an effect on the morphology of the as- prepared particles obtained by spray pyrolysis. By changing the solvent, the physical properties of the solution such as boiling point, solubility of salts, and spreading behavior of droplets on the substrate will change [50]. Since the boiling point of the water (100 °C) is higher than that of the ethylene glycol dimethyl ether (85 °C), the morphology of the film made from aqueous solution is less porous compared to the organic solution. In fact, slower evaporation of solvent during the droplet transport and results in slower

precipitation providing more time for the droplet to spread on the substrate. Therefore, the optimal spray parameters usually differ considerably for each type of solution.

Organic route based on metal-organic precursors and organic solvent with lower decomposition temperatures seems to be more favorable to improve morphology and compositional homogeneity. In fact, the organic route has the advantage of easier control over size or even the shape of the particles through changing the spray parameters. However, this is a rather costly process which can be resolved by replacing cheaper metal organic compounds. Since the precursors only need to be soluble in the solvent and must decompose into oxides at the deposition temperature, there would be extensive choice of organic precursors and solvent.
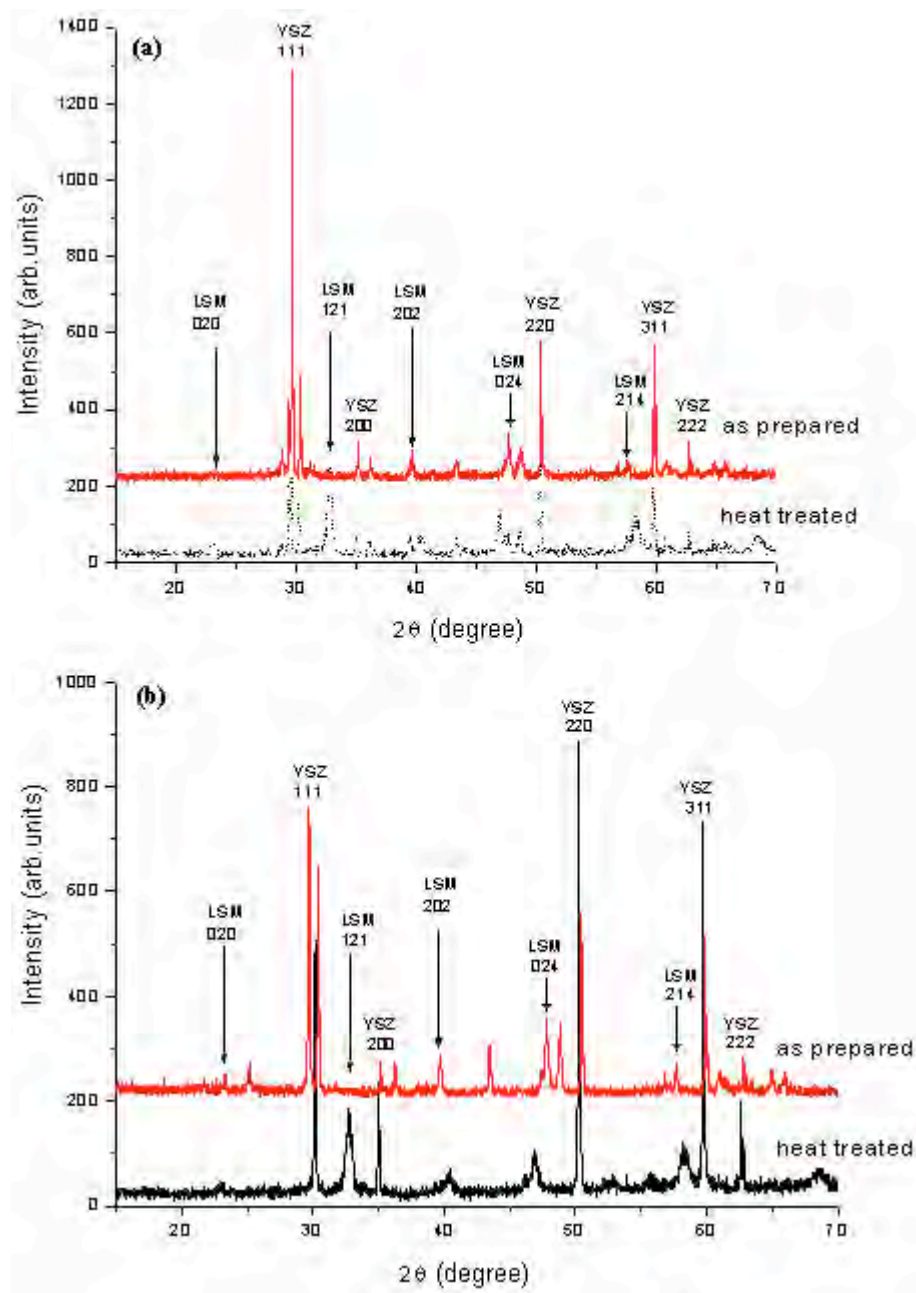
Fig. 4.2. The XRD spectra of samples produced in stage A from (a) aqueous and (b) organic solvents before and after heat treatment.

4.2. Investigation of Effect of Spray Parameters on the Microstructure of LSM Film

4.2.1. Effect of temperature and nozzle-to-substrate distance

The main objective of this part of the study is to understand the influence of spray parameters on the porosity of the LSM film. As discussed before, the substrate temperature is the most effective parameter in controlling the morphology and microstructure of the deposited film since the dynamics of the evaporation and decomposition reactions are strongly temperature dependent [50, 66, 67]. Using the metal-organic solution, the samples were made at different temperatures to find the appropriate range for thin film deposition. The specifications for sample preparation are listed below:

Organic solution:
Precursor: 80.3mg Tris Lanthanum, 22.7mg Bis Strontium, 100.7mg Tris Manganese,
Solvent: 50ml, Ethylene glycol dimethyl ether
Temperature: 300 °C
Oxygen/Nitrogen flow rate (ml/min): 80/800
Solution flow rate: 0.73 (ml/min)

At different temperatures from around 300 °C to 600 °C, the deposition process would follow what is shown in previous chapters (Fig. 2.8) and repeatedly in Fig. 4.3.
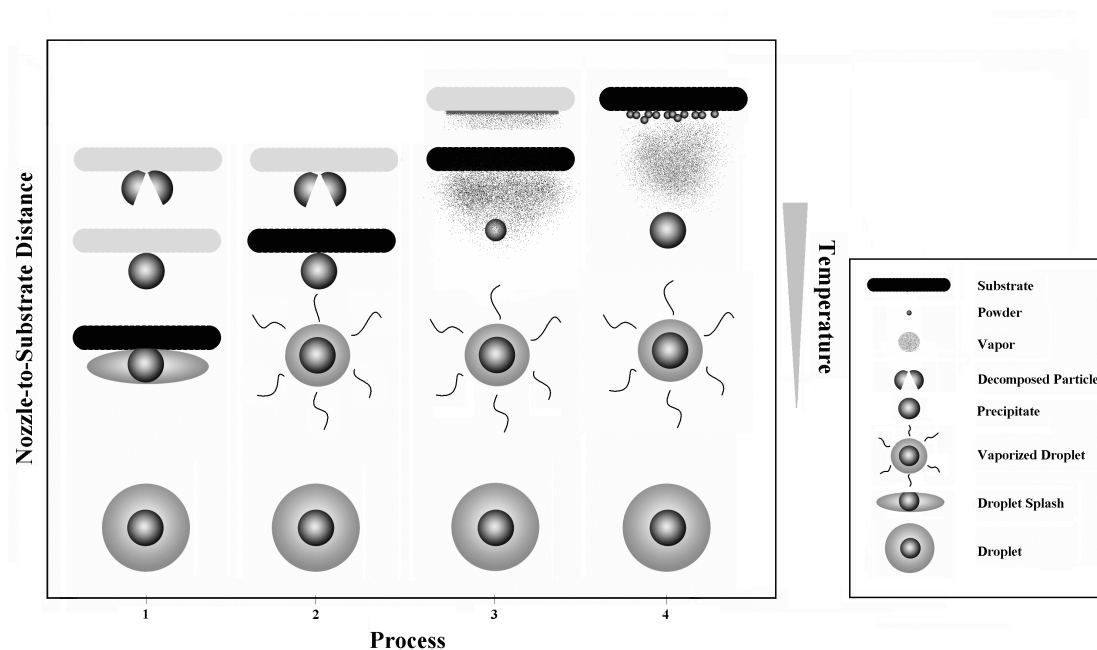
Fig. 4.3. Schematic depicting different deposition processes that occur as the nozzle-to-substrate distance and deposition temperature change.

The effect of temperature can be assumed to what happens similarly during change in nozzle-to-substrate distance. Considering the nozzle-to-substrate distance constant at position that there is more chance to obtain a thin film from deposition, at very low temperatures around 300 °C, the droplet approaches the surface without losing the surrounding liquid via vaporization. Therefore, it splashes on the surface of the substrate (as shown in process 1 in Fig. 4.3) allowing the solid solute to spread out over the surface. The resulting film structure will include large circles of the solid amorphous regions which are embedded uniformly over the surface. SEM micrographs shown in Fig. 4.4 reveal this effect.
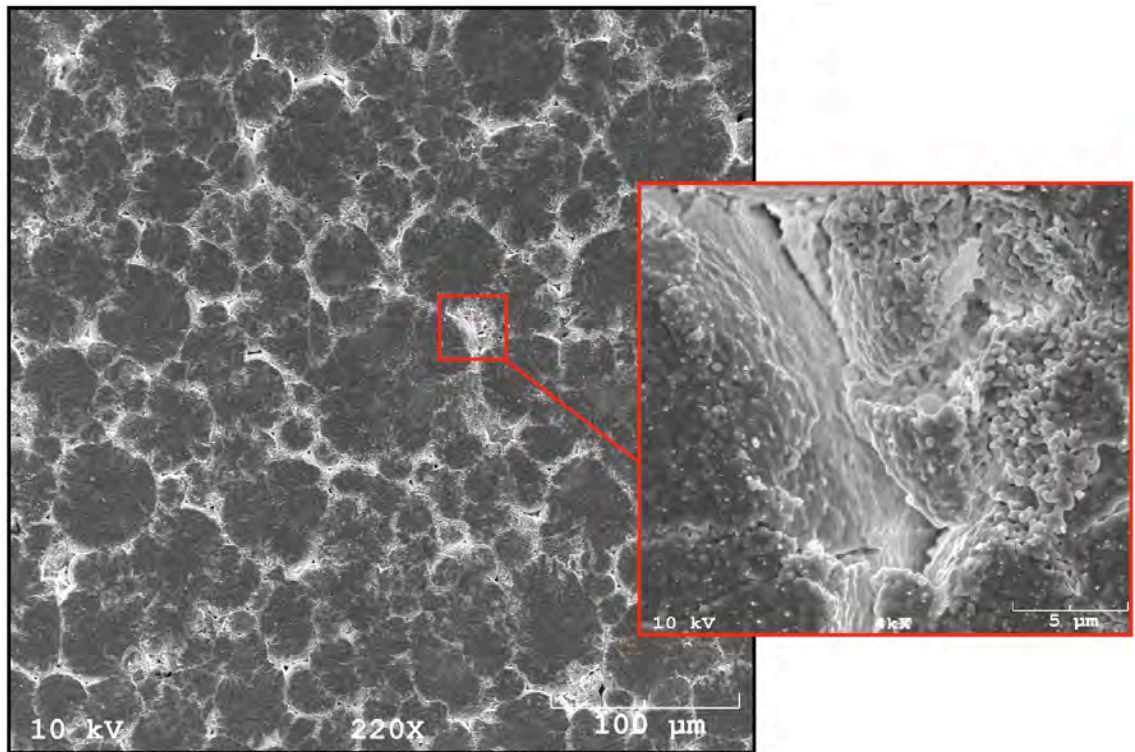
Fig. 4.4. SEM micrograph of the LSM film deposited at low temperature (300 °C) showing a dense amorphous film consisting large circles that are formed splashed droplets on the surface.

In this mode, a post-heat treatment process is required to enhance amorphous-to-crystalline transformation.

As the temperature increases, the droplet finds less time to spread over the surface and the solvent vaporization takes place faster. As a result, unshaped lumps of solid particles consisting of large pores will form throughout the surface. Increasing the temperature to 500 °C will result in pore growth and formation of solid islands within the film as shown in Fig. 4. 5.b.
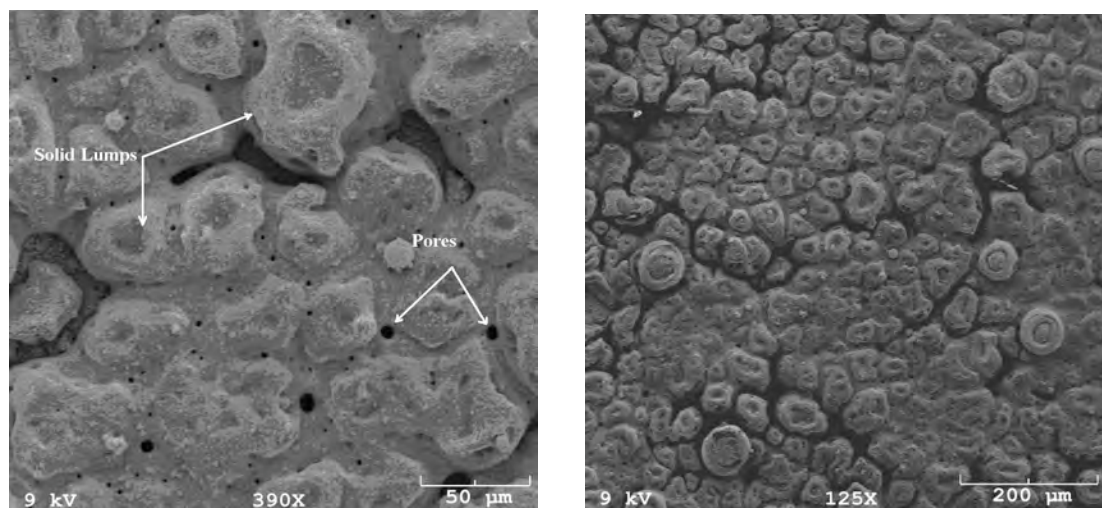
Fig. 4.5. SEM micrograph of the LSM film deposited at low temperatures (a) 480 °C and (b) 500 °C, showing growth of large holes between solid lumps leading to the formation of solid islands.

Results of the preliminary study on determination of the appropriate temperature range for achieving a thin film reveals that the deposition temperature has to be at least 520 °C to get a uniform dense layer. The effect of increasing the deposition temperature over 500 °C follows process 2 and 3 in Fig. 4.3 which is explained in detail in the following section. However, at temperatures above 600 °C, the solution rapidly vaporizes and the compound transforms to the vapor state before it reaches the substrate and the

chemical reaction takes place in the vapor phase resulting in formation of powdery particles. The same effect is observed when the substrate is located far from the spray nozzle as shown in process 4 in Fig. 4.3. This effect is explained in this section since the microstructural changes follow the same processes as in Fig. 4.3. Demonstrated in Fig. 4.6, is a typical example for understanding the influence of nozzle-to-substrate distance on the film microstructure.
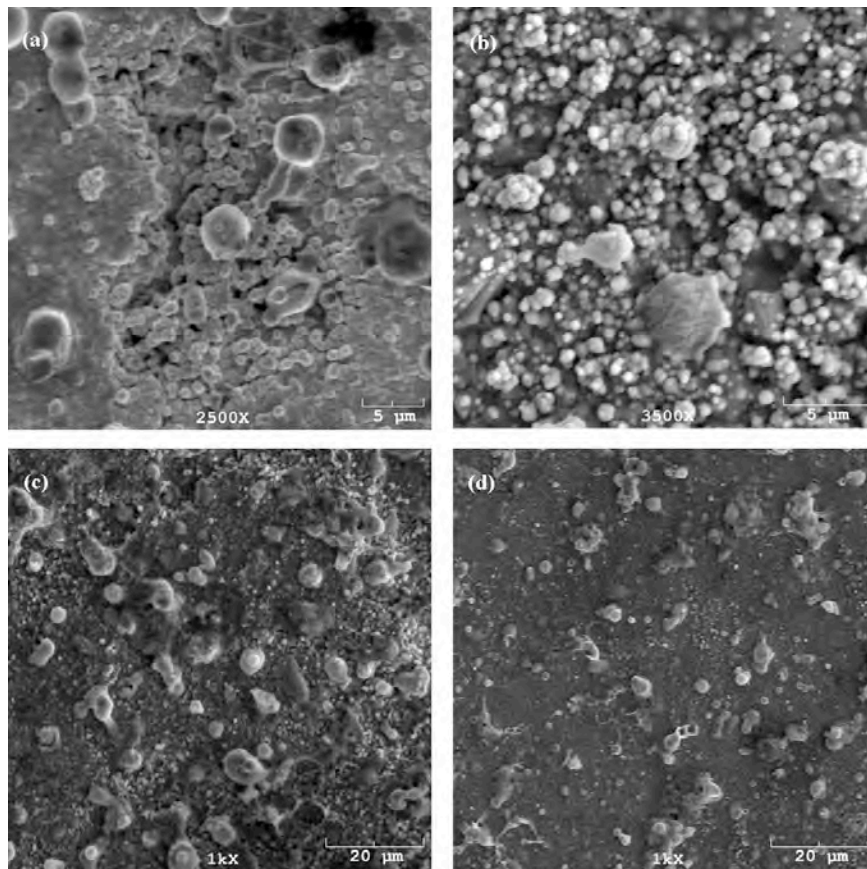

Fig. 4.6. Effect of nozzle-to-substrate distance on the microstructure of the LSM film, (a) 3.8, (b) 5.1, (c) 6.4, (d) 7.6cm.

Here, deposition is performed at 540 °C, at the solution flow rate of 1.13 ml/min and at the same conditions as the previous sample. The distance between the spray nozzle and the substrate was varied within the range of 3-8 cm. Although the effect is rather dependent on the other deposition parameters, the surface morphology of the films

produced at different distances have shown to be not critical [68]. It is clear that the effect of nozzle-to-substrate distance on the film microstructure is roughly in agreement with the types of processes depicted in Fig. 4.3. However, it is important to identify the distance at which deposition ends up with formation of a film. At short distance, the substrate is completely covered by an almost dense layer of the film when it is close to the spray nozzle. At further distance, particles are dispersed on the surface while they gradually lose their connectivity and tend to form powder. Moreover, at longer distance, only a small portion of droplets can reach the surface of the substrate and therefore the spray efficiency is considered to be low.

Fig. 4.7 shows the SEM cross sections of the samples in terms of changing the deposition temperatures and the solution flow rate in comparison. Effective microstructural properties in terms of film porosity and morphology are determined to be more affected by the temperature and solution flow rate. This tabular figure demonstrates the variety of dense to porous microstructures that could be achieved via changing the temperature and solution flow rate. Regardless of the influence of the solution flow rate, formation of uniform dense layers is observed at 520 °C and increasing the temperature to 540 °C does not make significant changes in porosity. At 540 °C and at flow rate 1.13 ml/min an almost perfect CVD–like layer can be also obtained. However, as the temperature increases to 560 °C, porous microstructure is gradually appeared. The most significant changes in microstructure at each solution flow rates are observed to be related to higher temperatures. In fact, higher deposition temperatures help to decompose the precursors and result in formation of highly porous film. The deposition process is in fact following processes 2 and 3 according to Fig. 4.3. The solvent evaporates before the

droplet reaches the surface and the decomposition occur upon the precipitates hit the surface. Further increasing the temperature may lead the solvent to vaporize as the droplet approaches the substrate and then the solid vapor diffuses to the substrate to undergo a heterogeneous reaction there. However, it is difficult to distinguish which process is dominating at an exact temperature and flow rate since both processes can occur simultaneously in the temperature range of 560-580 °C. As mentioned before, high temperatures over 580 °C resulted in no reasonable deposition. This is related to gas phase nucleation which can usually produce nano-powders that will not deposit on the YSZ and may be carried away by the carrier gas.

4.2.2. Effect of solution flow rate

The effect of solution flow rate is emerged in Fig.4.7. It appears that the solution flow rate is an important parameter in controlling the microstructure since it is associated with the amount of energy that is given to the droplet to travel toward the substrate. The effect of temperature is even more pronounced if the solution flow rate is increased. As Fig. 4.7 shows, the film deposited using the lower solution flow rate of 0.73 ml/min looks slightly denser than those deposited at higher solution flow rate, particularly, at low temperature. Increasing the solution flow rate leads to formation of much thinner layers at lower temperatures, since it does not give enough activation energy and time to decompose the precursors. Therefore the spray and vapors are transported by the carrier gases away from the substrate. However, increasing the solution flow rate at high temperatures will cause rapid deposition of a larger number of aerosol droplets. In other words, higher flow rate leave less time for the droplet to spread over the substrate leading

to formation of a more agglomerated porous structure. This effect is more enhanced between 560-580 °C. Therefore, if the solution flow rate and the temperature are in the optimal range with respect to each other, the microstructure and porosity of the film can be controlled.
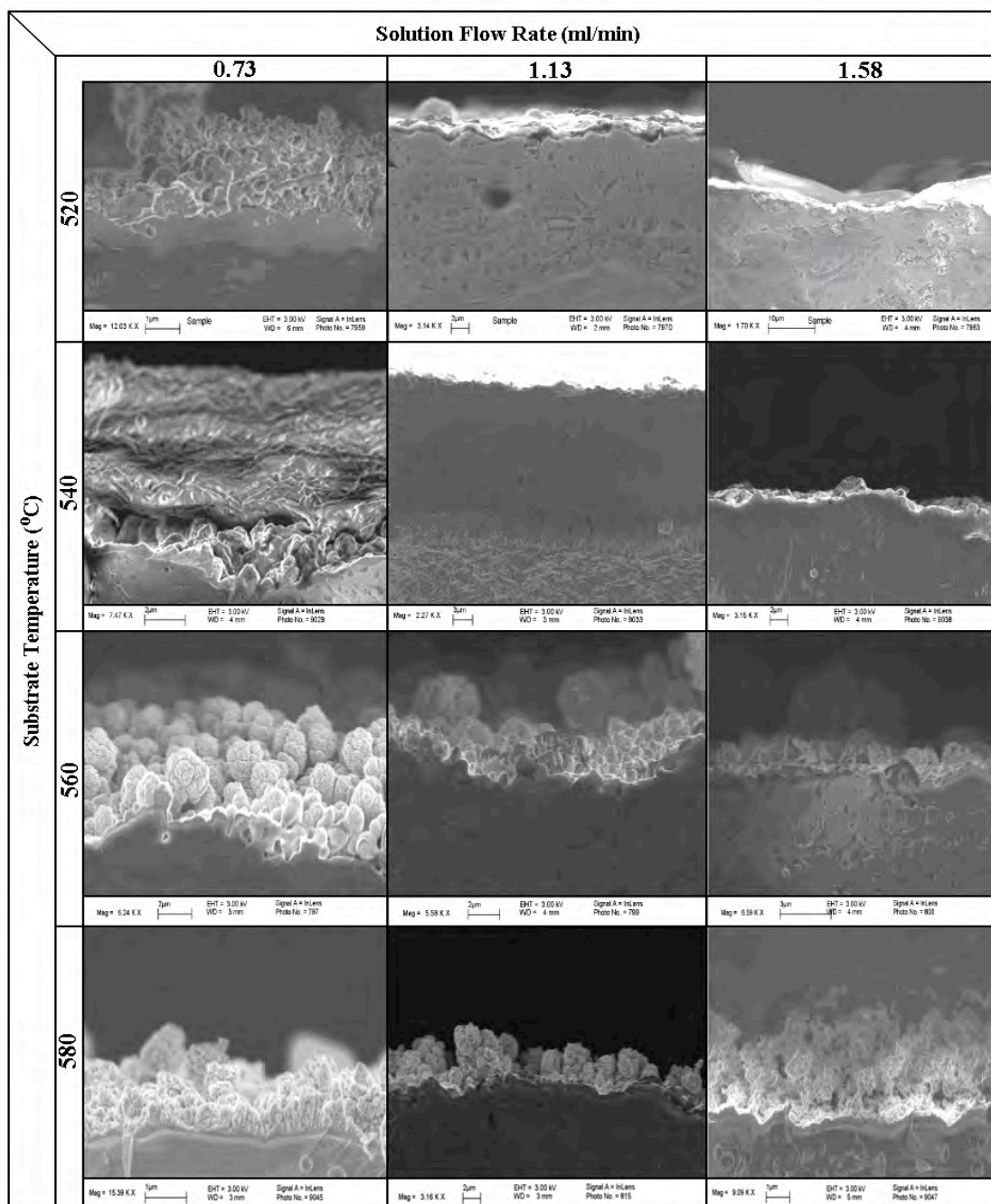
Fig. 4.7. The effect of temperature and the solution flow rate on the microstructure of the LSM cathode film deposited on the YSZ electrolyte.

4.2.3. Effect of carrier gas concentration (oxygen flow rate)

In order to investigate how the amount of oxygen in the carrier gas affects the film morphology, deposition of the LSM film on YSZ substrate was performed at 4 different oxygen/nitrogen gas flow ratios by keeping the rate of nitrogen gas fixed at 800 ml/min and increasing the oxygen flow rate from 0 to 80, 160 and 240 ml/min. It has been reported by Abrutis et al that increasing the amount of oxygen flow rate in the carrier gas flow results in formation of porous films of LSM with a disordered columnar structure. Depending on the oxygen concentration in the aerosol flow, films of dense or porous morphology can be obtained [69]. Result of our study is in agreement with what is reported in the literature.

It should be noted that in order to be able to analyze the change in the microstructure and study the trend of changing the microstructure with varying one parameter, other deposition parameters should be fixed during the experiment and their effects need to be assumed negligible during the investigations. The deposition condition is fixed for all oxygen flow rates as the following:

Organic solution:
Precursor: 80mg Tris Lanthanum, 30mg Bis Strontium, 90mg Tris Manganese,
Solvent: 50ml, Ethylene glycol dimethyl ether
Temperature: 540 °C
Solution flow rate: 1.13 (ml/min)

As shown in Fig. 4.8, a dense LSM film is formed without presence of oxygen in the gas flow, while a porous film consisting of large agglomerates of particles is obtained at the oxygen flow rate of 80 ml/min. As the oxygen flow rate is increased to 160 ml/min,

small particles start to grow in any direction and form crystalline branch-like structures with a large degree of porosity.
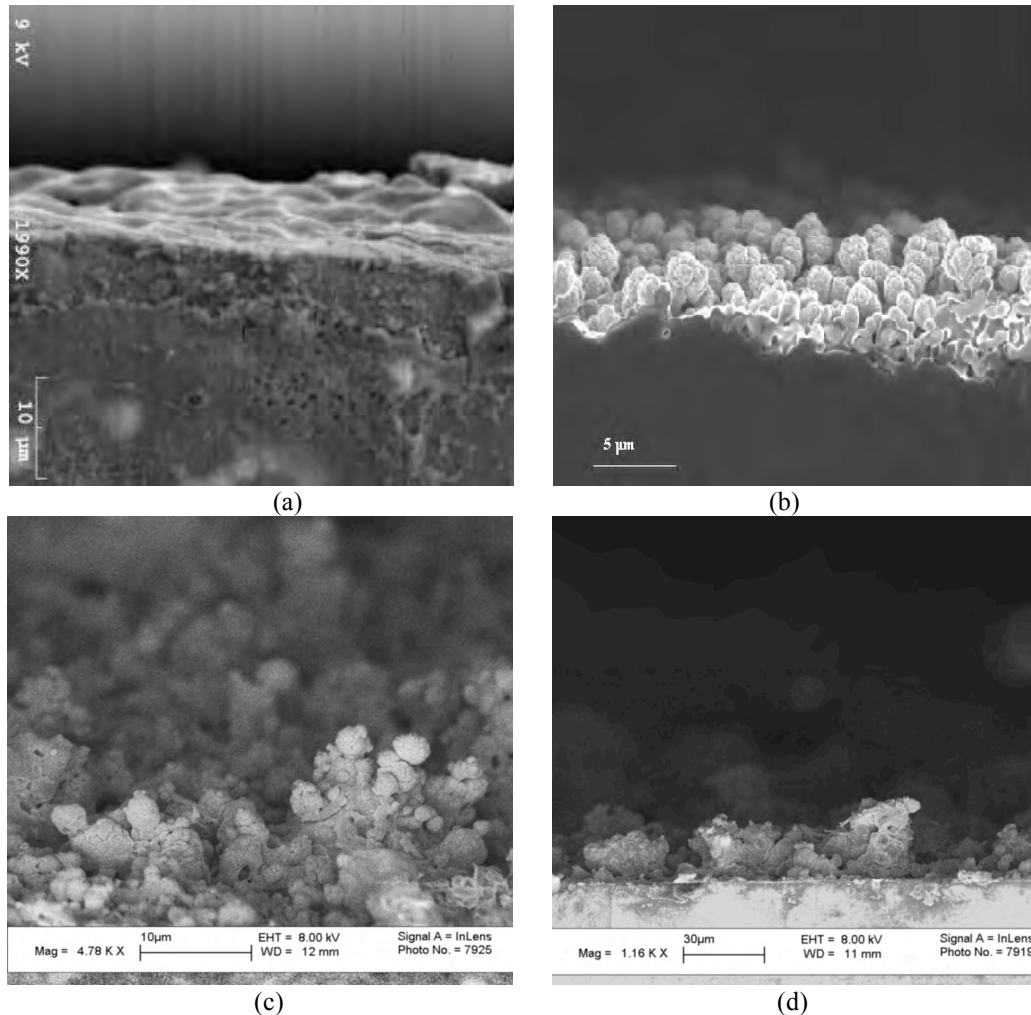

Fig. 4.8. SEM cross sections showing the effect of oxygen flow rate on the morphology and porosity of the LSM film ; (a) 0, (b) 80, (c) 120, (d) 240 ml/min.

Fig. 4.9 shows formation and growth of nanocrystalline particles inside large particles. The higher magnification image reveals well-ordered growth of small grains inside the large spherical particles. One possible reason can be attributed to the fact that the oxygen present in aerosol flow facilitates precursor decomposition and consequently increases the growth rate and changes the film growth mechanism to a disordered branch-like and columnar growth, as can be seen in Fig. 4.10.
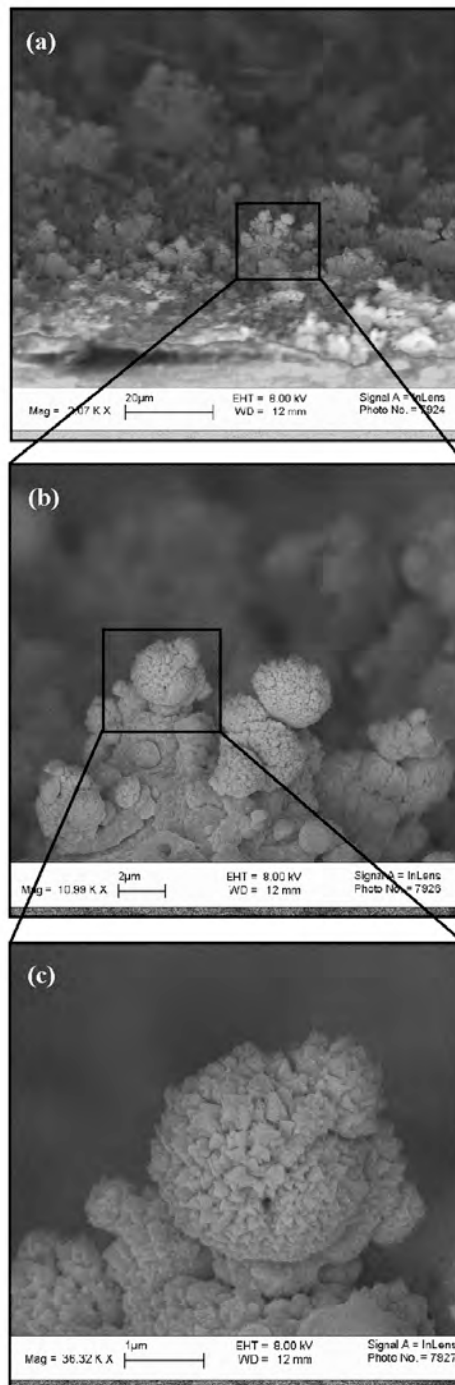
Fig. 4.9. The effect of oxygen gas concentration on the microstructure and morphology of the LSM cathode film deposited at 160 ml/min O$_2$ flow rate on the YSZ electrolyte.

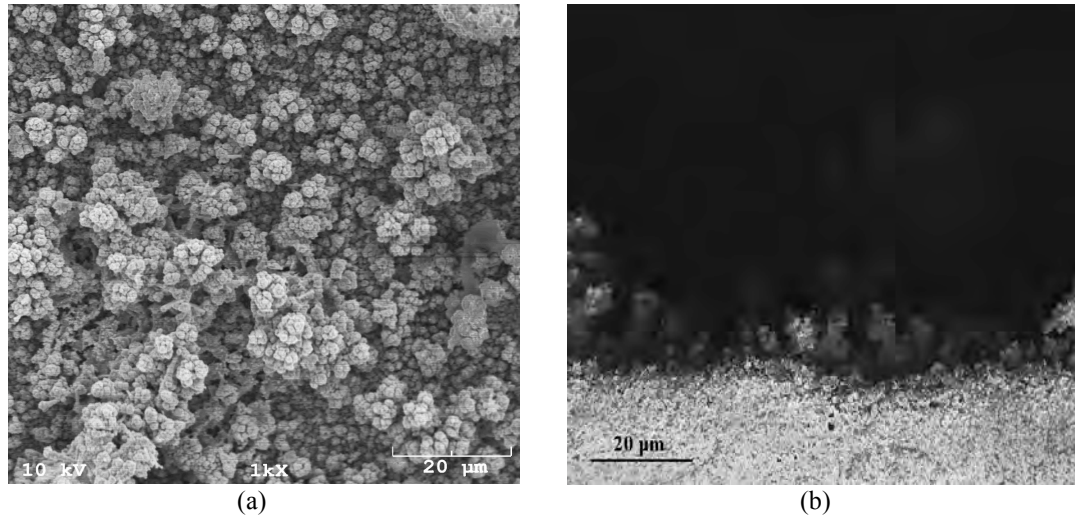<table>
<tr><td>(a)</td><td>(b)</td></tr>
</table>

Fig. 4.10. SEM (a) micrograph and (b) cross-section of the LSM sample deposited at 160 ml/min oxygen flow rate, showing the columnar growth with increasing the oxygen flow rate.

Fig. 4.11 shows the SEM cross-section of the LSM sample deposited at 160 ml/min oxygen flow rate, and the EDS dot mapping showing uniform distribution of Mn, Sr, and La on the cross-section surface.
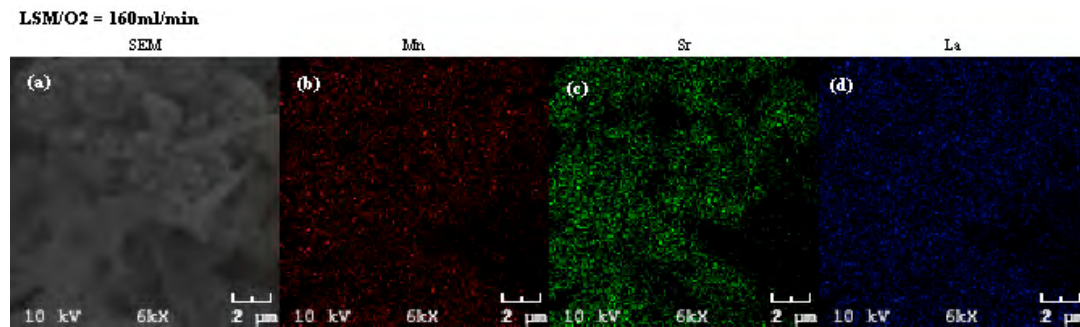

Fig. 4.11. (a) SEM cross-section of the LSM sample deposited at 160 ml/min oxygen flow rate, and EDS dot mapping showing (b) Mn, (c) Sr, and (d) La distribution on the cross-section surface.

Increasing the oxygen flow rate to 240 ml/min resulted in formation of very large agglomerates that are embedded on the surface without forming any specific morphology

(Fig. 4.12). The effect can be correlated to that the high gas flow rate dominates the favorable influence of presence of oxygen and shortens the residence time resulting in decreasing the film crystallinity. Consequently, the oxygen gas flow rates below 160 ml/min result in a reasonable deposition with variety of dense to porous morphologies. Based on these results, the oxygen gas flow rate of 80 ml/min is chosen for deposition of the graded film, since presence of a uniform columnar microstructure associated with this flow rate is more desirable for enhancing the gas transport properties in the cathode film.
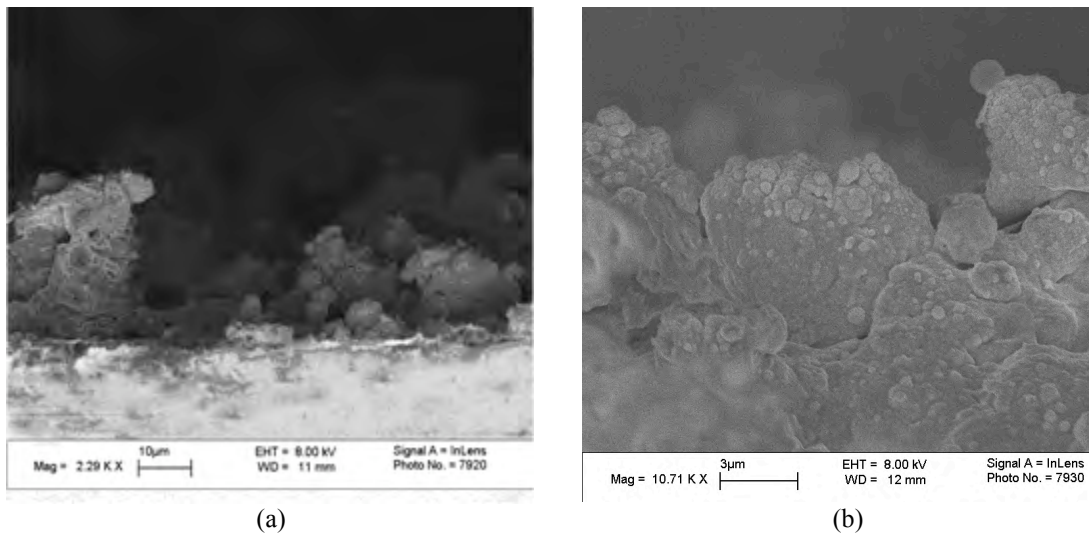

(a)   (b)

Fig. 4.12. SEM cross sections of the LSM sample deposited at 240ml/min oxygen flow rate, (a) 10 µm magnification; (b) higher magnification image reveals the large agglomerates of particles formed on the surface.

4.2.4. Effect of precursor solution concentration

The precursor solution concentration should be as high as it results in a reasonable deposition rate. However, concentrations should not be higher than the salt solubility limit. Here, the size and morphology of particles in the films showed to be dependent on the precursor solution concentration while all the other parameters are constant. Significant changes in the particle size can be observed at the low and high ends of

changing the solution concentration. From the SEM cross sections (Fig. 4.13a), at high concentration (0.5 M) large particles with a high degree of agglomeration were formed while smaller particles resulted at low concentration (0.1 M) as in Fig. 4.13b. High porosity was also observed at high concentration which is attributed to the formation of large particles with a high degree of agglomeration. At low concentration, the film consisted of a dense layer with highly crystalline nanosized particles that were embedded orderly on the surface.
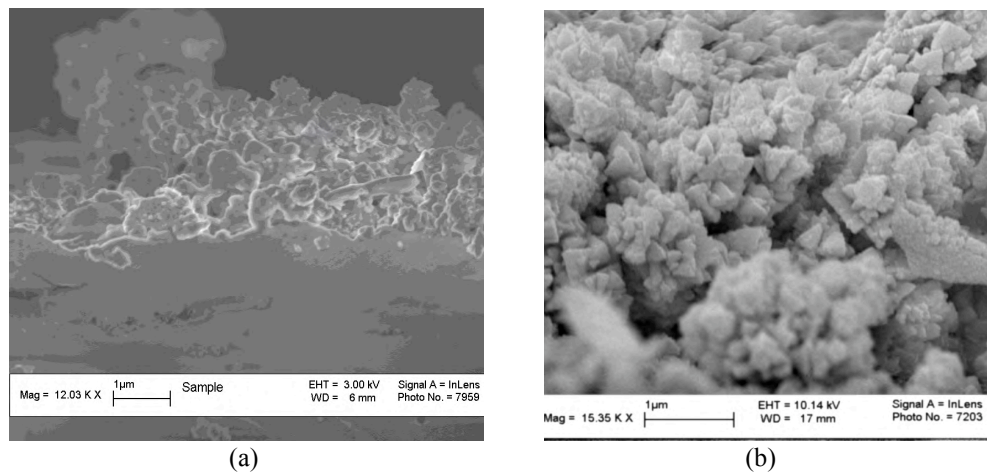

(a)   (b)

Fig. 4.13. SEM cross sections of the LSM film deposited from (a) high and (b) low concentration precursor solutions.

4.3. Deposition of Gradient Porous LSM Film

Based on the results of previous sections on the effect of deposition parameters on the microstructure such as temperature, solution flow rate, etc., a gradient porous microstructure is achieved in this part of the work by applying a multiple-step spray deposition consisting of changing the precursor solution concentration, deposition temperature and solution flow rate in the reasonable range. The overall results of the previous sections are summarized in the following table. Fig. 4.14 shows the image of the real gradient porous LSM sample, one layer coating of LSM, and YSZ un-coated substrate. Black color of the gradient porous LSM is indicative of the crystallinity of the LSM phase, while the grey color of the one layer LSM coating corresponds to the lower degree of crystallinity.

Table 4.1. Spray conditions for three experimental stages.

Stage	Condition Solvent	Precursors (mg)			Solvent (ml)	Temperature (°C)	Solution flow rate (ml/min)	Pyrolysis process	LSM film composition	YSZ electrolyte
A	Aqueous	Lanthanum acetate	Strontium acetate	Manganese acetate	Water	480	0.73	Endothermic (vaporization)	Inhomogeneous	Crack growth/YSZ failure
		110.6	30	86	25					
	Organic	Tris Lanthanum	Bis Strontium	Tris Manganese	Ethylene glycol dimethyl ether	480	0.73	Exothermic	Homogeneous	No cracks
		80.3	22.7	100.7	25					
B	Organic	80.3	22.7	100.7	25	520,540,560,580	0.73, 1.13, 1.58	Exothermic	Homogeneous	No cracks
C	Organic	Tris Lanthanum	Bis Strontium	Tris Manganese	1-2 Dimethoxyethane					
		180	60	160	100	520	0.73		Nanocrystalline fine interlayer	
		360	120	320	50	540	1.13	Exothermic	Gradient	No cracks
		360	120	320	50	560	1.13		porous	
		360	120	320	50	580	1.58		coarse layers	

The ideal goal of achieving optimal properties in cathode is described as having a fine layer close to the surface of electrolyte and the gradually coarser outer layers. The structural changes associated to each deposition condition have been discussed in detail earlier. As it is shown in Table 4.1, starting with spraying a dilute solution (0.1 M) at low

substrate temperature of 520 ºC and with a low rate of spraying the solution (0.73 ml/min), a sufficient time would be provided for surface reactions and for deposition of particles in a proper arrangement to produce a uniform interlayer between electrolyte and the porous electrode. By increasing the temperature to 540 ºC and the solution flow rate to 1.13 ml/min, gas phase nucleation creates smaller particles embedded in the first layer produced through the first process, creating more porous structure. Here, higher concentrated solution (0.5 M) allows deposition of more particles in a random manner. In the third stage, the solution flow rate is kept constant at 1.13 ml/min; however, the temperature is increased to 560 ºC to help more decomposition of the precursors. In the fourth and last stage, we expect to have a layer with higher porosity in which the particles may slightly start to grow. Increasing temperature to 580 ºC along with increasing solution flow rate to 1.58 ml/min will result in fast evaporation of highly concentrated solution and lack of time for solute diffusion and particle densification resulting in highly porous films [70]. Fig. 4.15 depicts the plot of electrode thickness that is determined from SEM cross-section micrographs as a function of deposition time at each deposition step. The rate of deposition increases as a function of solution flow rate and deposition temperature.
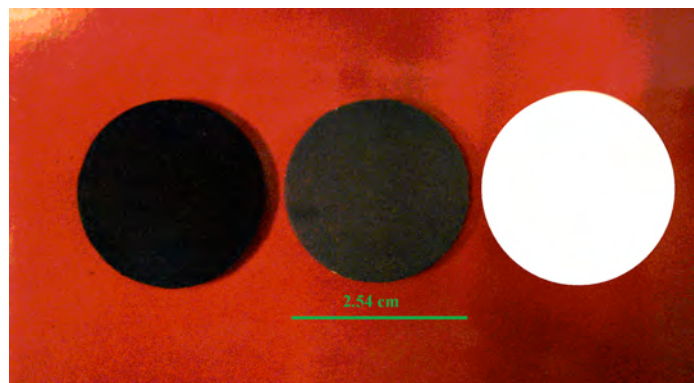
Fig. 4.14. Left to right: gradient porous LSM, one layer coating of LSM, and YSZ un-coated substrate. Black color of the gradient porous LSM is indicative of the crystallinity of the LSM phase.
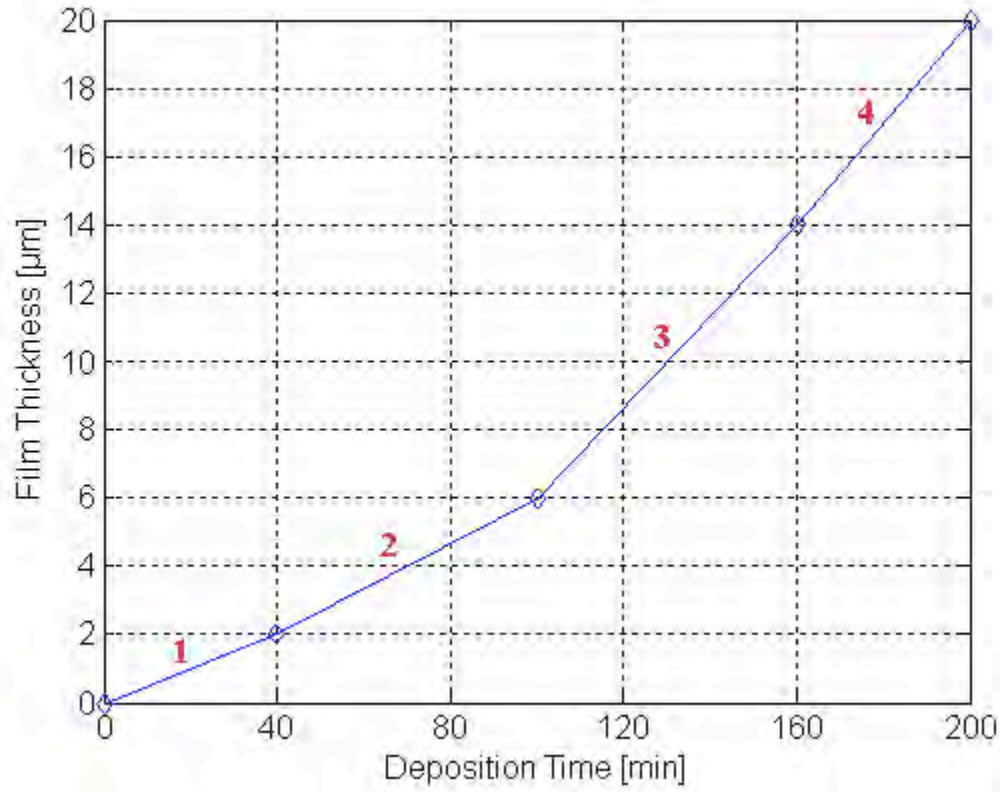

Fig. 4.15. The plot of the first gradient cathode film thickness as a function of deposition time. The film thickness increases drastically by changing the deposition parameters. The thicknesses were determined from SEM cross-section micrographs.
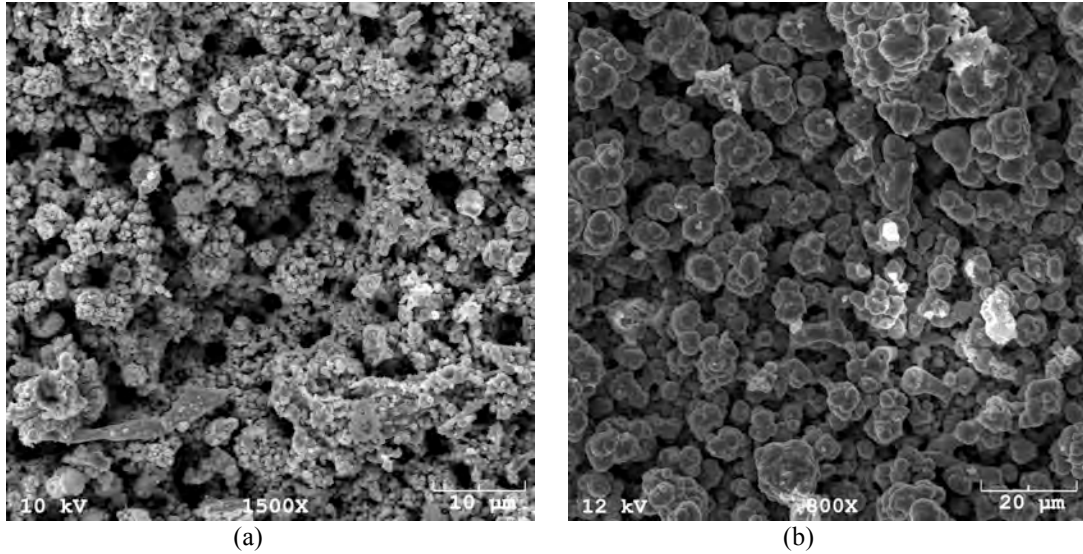
<div align="center">(a)   (b)</div>

Fig. 4.16. SEM micrographs of the gradient porous LSM sample, (a) before heat treatment and (b) after heat treatment.

Fig. 4.16 reveals the effect of post-heat treatment on the microstructure of the gradient porous LSM film. The outset layer on the surface as it is seen in Fig. 4.16.a is formed through uniform deposition of submicron droplets of spherical shapes creating quite large pores of narrow size distribution between 1-5 μm. However, a large portion of the porosity is attributed to the nanosized pores. Here, the annealing temperature of 700 °C has led to partially growth and agglomeration of the particles resulted in a more uniform microstructure. However, if the particles undergo higher temperature sintering, fine pores will be filled and they will be no longer available due to further grain growth.

Fig. 4.17.a shows the gradient porous LSM cathode with the average thickness of ~20 μm. However, the SEM cross section of the heat treated LSM film in Fig.4.17.c shows that the film thickness has reached to approximately 100 μm. Variation in the film thickness is one of the drawbacks of the spray technique and is pronounced here due to the angular position of the substrate with respect to spray direction. However, this effect can be mitigated by putting the substrate on a rotary holder so that the aerosol droplets

can reach every spot on the surface and create a more uniform film. The substrate rotation has been performed during the second set of experiment for processing the gradient porous LSM film which is discussed in section 4.3.3.

Overall, the LSM film is compositionally homogeneous and crack-free with a semi-columnar porous structure. Scotch tape test results showed high cohesive strength of the film as no peeling off was observed and the LSM film was well adhered to the YSZ substrate. Fig.4.17.b (as the negative image of Fig.4.17.a) reveals the porosity gradient in 4 deposited layers in detail; here, the cathode microstructure consists of a nanostructured thin interlayer on the surface of the YSZ substrate and gradient porous outer multi-layers. The coarse top layer consisting of the large interconnected pore channels allow gas transport to the inner layers while the inner layers consist of lower degree of porosity to provide film integrity. At the interface layer, as the particles get smaller, a larger number of triple phase boundaries (TPB) as the three-dimensional sites between LSM particles, YSZ electrolyte and gas-phase (O_2) or electrode surface sites along with higher porosity can be developed resulting in increasing the cathodic activity. Reports show that nanostructured electrodes dramatically reduce electrode/electrolyte interfacial polarization resistances and improve cell performance supporting that the microstructure close to the interface should be as fine as possible [26, 39]. However, smaller particles can not always guarantee a higher activity since they are more capable to grow and to be sintered at working temperatures in real cell and fill the active sites [71]. At the interface with YSZ, a thin uniform nanostructured active LSM interlayer with crystallite size smaller than 100 nm is observed.
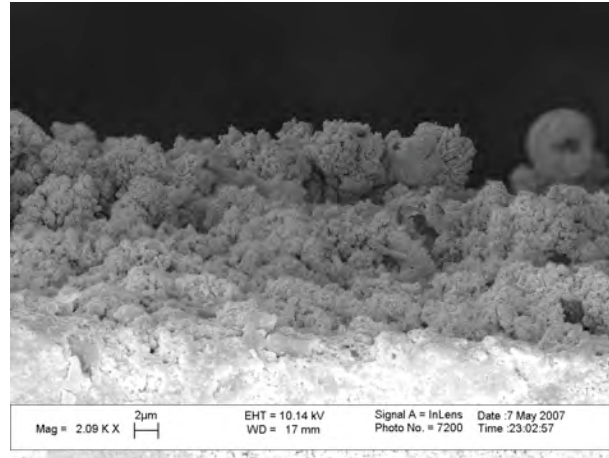
(a)
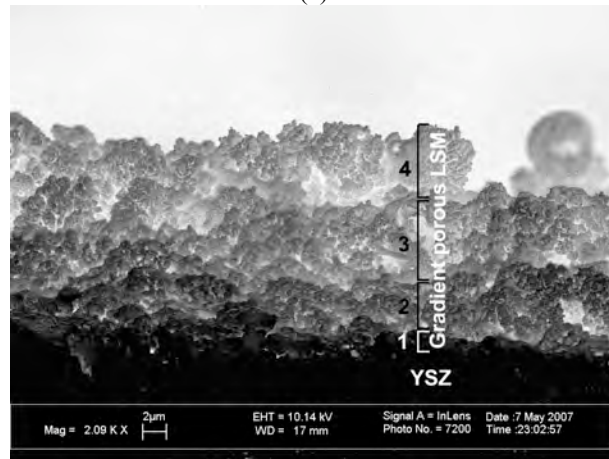
(b)
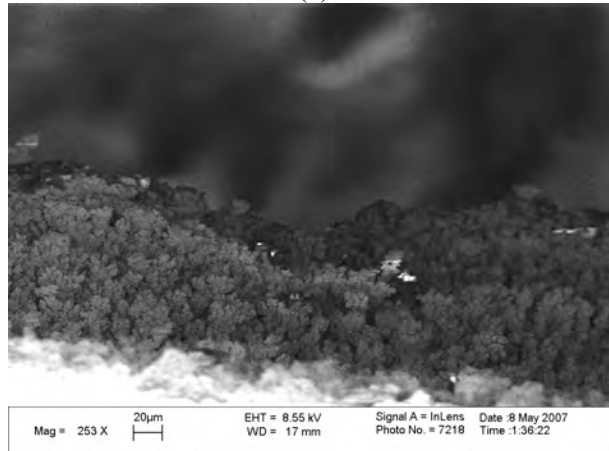
(c)

Fig. 4.17. (a) SEM cross-section image of the gradient porous LSM made by multiple spray pyrolysis depositions. (b) Negative image of a. (c) SEM cross section of the gradient porous LSM after heat treatment.

The presence of nanocrystalline interlayer is expected to enhance the exchange rate of oxygen between the gas-phase and the solid phases offering an extremely high surface area for oxygen reduction. The oxygen mass transport is expected be enhanced through the uniform nanostructure layer by rapid diffusion via enhanced grain boundaries of the nano-sized grains in the thin layer [14, 72].

The SEM cross section of the heat treated sample indicates the branch-like microstructure as well as partially grain growth, leading to decreasing the number of open pores (Fig. 4.17.c). Thus, by eliminating the heat treatment and sintering stage in spray pyrolysis technique, the desired amount of porosity could be retained in the microstructure.
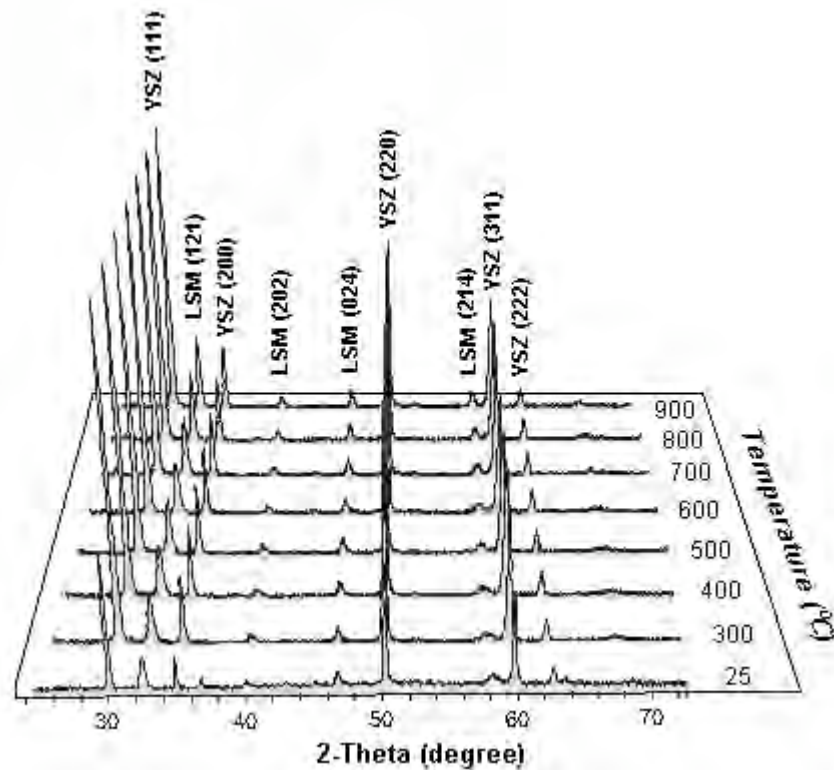

Fig. 4.18. Temperature-dependent XRD of the gradient porous LSM thin film deposited on YSZ substrate which confirms phase stability of the film at operating temperatures (700-900 °C).
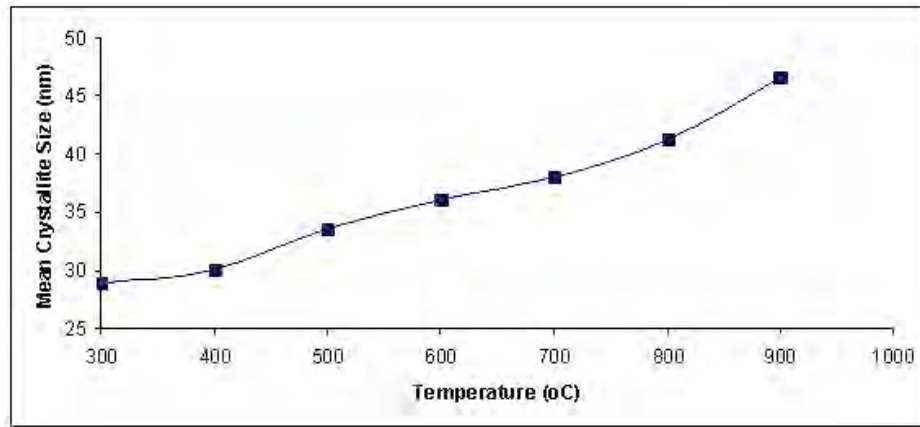
Fig. 4.19. Relationship between LSM mean crystallite size and temperature.

Fig. 4.18 shows the temperature-dependent XRD patterns of the gradient porous LSM thin film deposited on YSZ substrate during heat treatment. Final phases of the LSM film show slightly sharper peaks meaning a small increase in crystallinity and crystal growth during heat treatment. Although crystallinity is slightly improved, no phase degradation is observed at elevated temperatures. The black color of the as-prepared LSM film was also comparable to that of heat treated sample, which confirms formation of crystalline phases during deposition. This result not only demonstrates the capability of spray pyrolysis for producing highly crystalline LSM phase at 520-580 °C without need for subsequent heat treatment, but also confirms phase stability of the cathode film at higher operating temperatures (700-900 °C). The mean crystallite size of the LSM film (D) was obtained from the Scherrer formula:

$D = 0.9\lambda / \beta \cos \theta$ *(4.1)*

where $\lambda = 1.541$, θ is the diffraction peak angle, and β denotes the full width at half maximum (FWHM) of the corresponding diffraction peak. Here, (121) plane peak as the main single peak of LSM was used to calculate crystallite size. Fig. 4.19 shows the LSM average crystallite size of ~25 nm at 300 °C which slightly changes to ~50 nm by increasing the temperature to 900 °C. Such small variations in crystallite size of the LSM cathode during heating up to the range of operating temperatures confirms that the spray pyrolized gradient film fabricated at the temperature range of 520-580 °C is composed of highly crystalline LSM phase before undergoing further heat treatment. Thus, this is an advantage of the spray pyrolysis for processing stable optimal microstructures at much lower temperatures than the conventional processes and without need for further heat treatment.

<table>
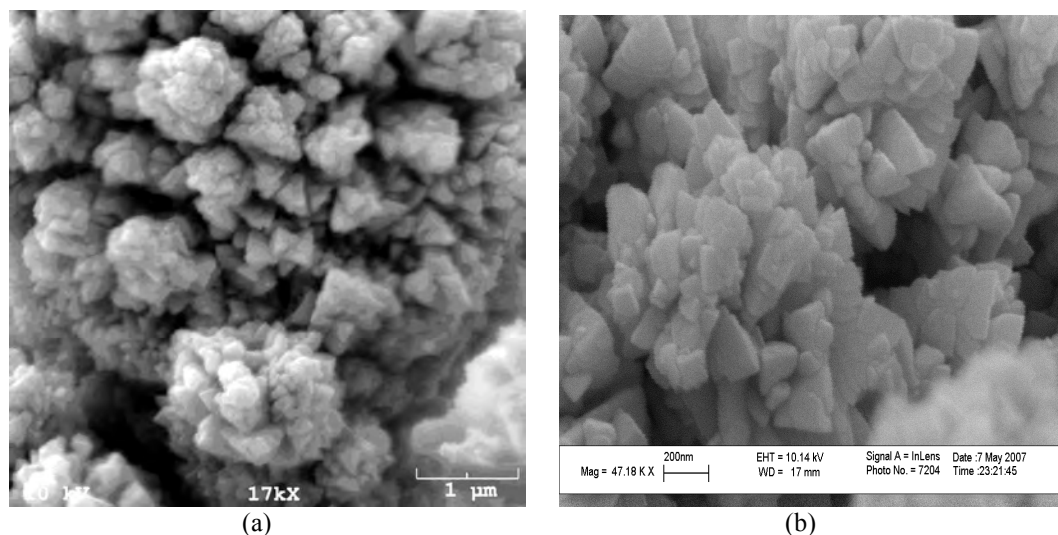<tr><td>(a)</td><td>(b)</td></tr>
</table>

Fig. 4.20. SEM cross section image of the active nanostructured interlayer, (a) before heat treatment and (b) after heat treatment.

Fig. 4.20 shows the SEM cross section images of the active nanostructured interlayer before and after heat treatment. Each particle consists of porous crystallites smaller than 50 nm and sintered to about 100 nm after heat treatment which is consistent with the average crystallite size calculated from Scherrer formula. EDX results showed

approximately the same molar ratio of the heat treated sample La:Sr:Mn = 0.70:0.24:1

with respect to as-prepared one. However, the precise stoicheometry of LSM is important

since any changes in elements content lead to changes in physical and chemical

properties of the cathode.

Fig. 4.21 shows the SEM cross-section of the gradient porous LSM sample and

the EDS dot mapping showing uniform distribution of Mn, Sr, and La on the 20 μm

cross-section surface. The elemental mapping indicates presence of compositional

uniformity and homogeneity over the whole microstructurally graded LSM film with

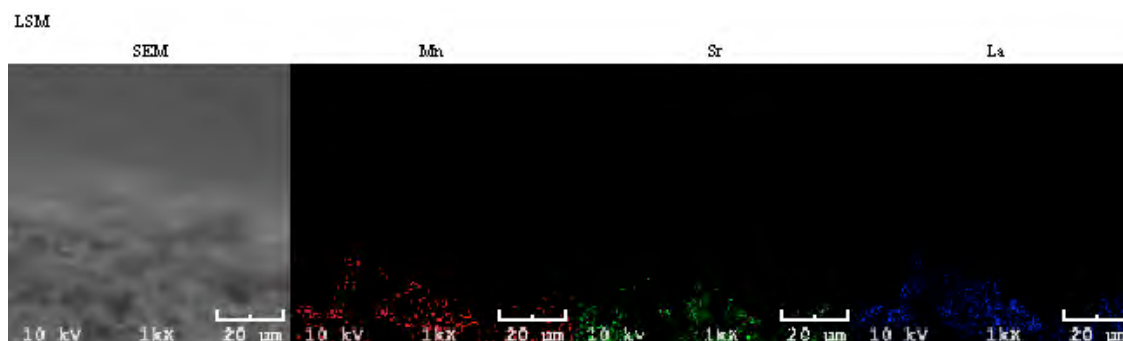layers produced at different processing conditions.

Fig. 4.21. (a) SEM cross-section of the gradient porous LSM sample deposited and EDS dot mapping showing (b) Mn, (c) Sr, and (d) La distribution on the cross-section surface.

Shown in Figure 4.22 are the adsorption isotherms of the gradient porous LSM

film as deposited on the YSZ substrate (coated sample) and the un-coated YSZ substrate.

The adsorption isotherms match each other for the portion of gas that is adsorbed on the

YSZ substrate. However, the extended part of the isotherm of the coated sample

corresponds to the portion of gas that is adsorbed on the porous coating. Fig. 4. 23 shows

the pore-size distribution for the coated and un-coated samples that was obtained using

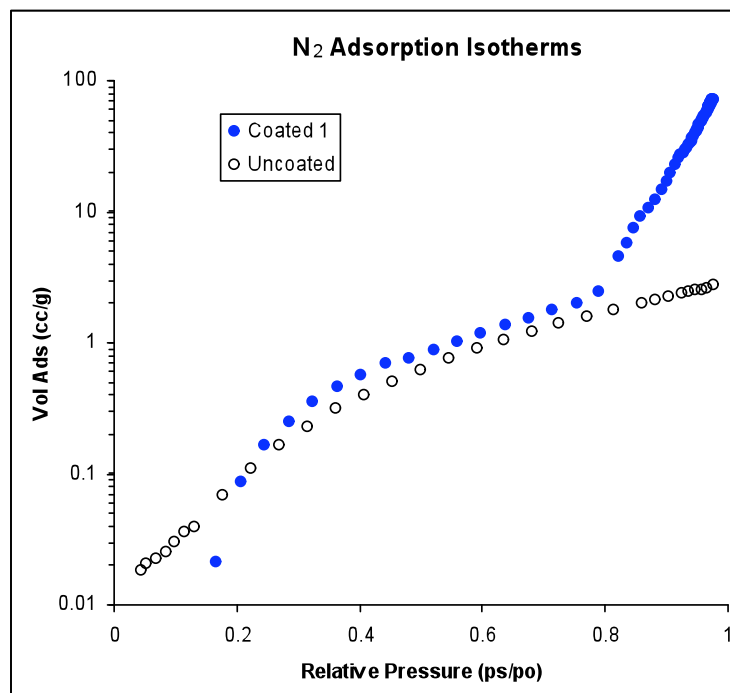N_2 adsorption measurements on samples degassed for 2 h at 250°C.

Fig. 4. 22. Nitrogen adsorption isotherms for the gradient porous LSM film deposited on YSZ and the un-coated YSZ substrate.
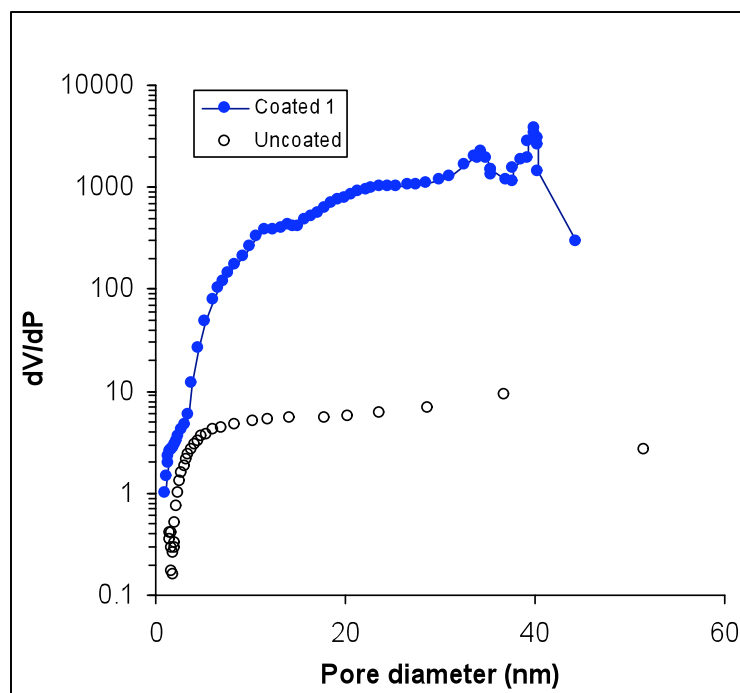

Fig. 4.23. Pore size distribution for the gradient porous LSM film deposited on YSZ and the un-coated YSZ substrate.

4.3. Reproducibility of Gradient Porous LSM Film

In order to study the reproducibility of the gradient porous film via spray pyrolysis technique, the same set of experiment was repeated to process the gradient porous LSM cathode. Fig. 4.24 demonstrates the SEM cross section image of the functionally gradient porous LSM cathode that is successfully produced on top of YSZ substrate. Results of XRD and EDS analysis shows that the LSM crystalline phase is completely achieved through this process. Therefore, spray pyrolysis technique can be utilized as a low temperature processing technique to produce highly crystalline functionally graded LSM cathodes without need for further high-temperature heat treatment.

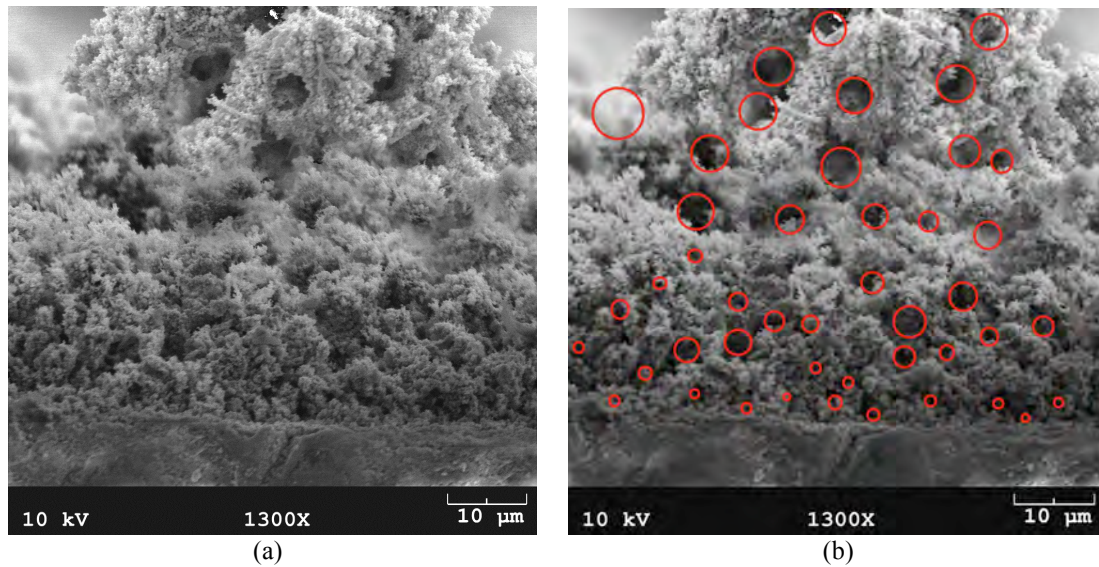(a)   (b)

Fig. 4.24. (a) and (b): SEM cross section image of the functionally gradient porous LSM cathode on top of YSZ substrate. Red circles show presence of large pores on the top layer and gradually smaller pores next to the electrolyte.
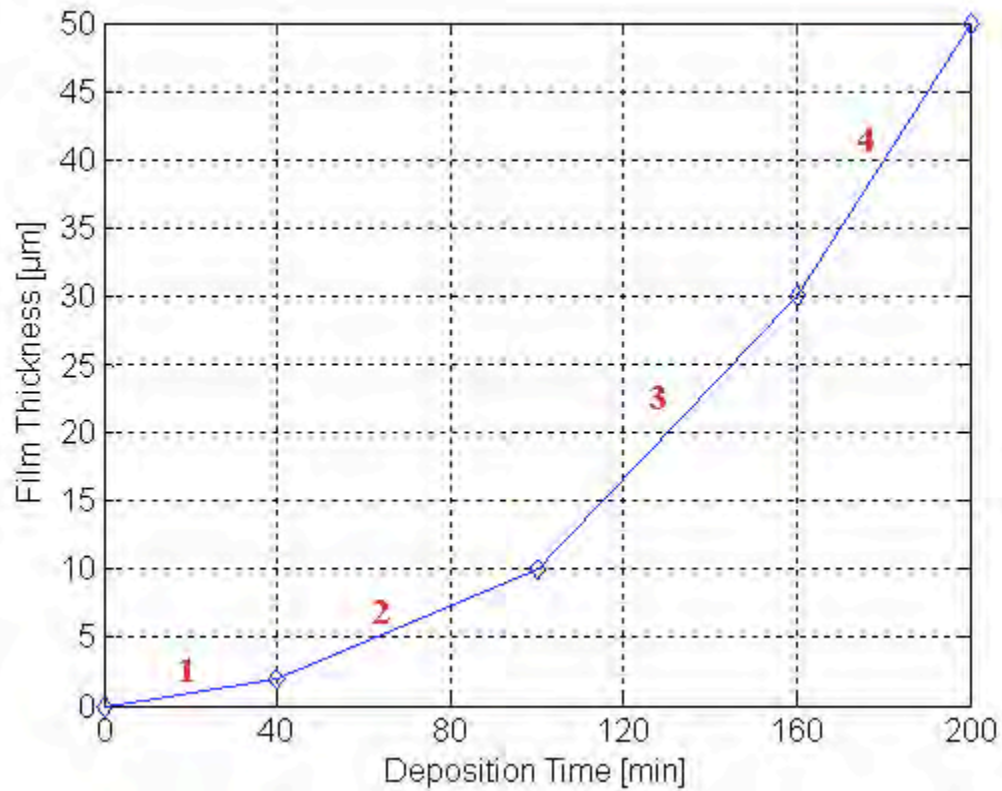
Fig. 4.25. The plot of the second gradient cathode film thickness as a function of deposition time. The film thickness increases drastically by changing the deposition parameters. The thicknesses were determined from SEM cross-section micrographs.

The thickness of the gradient LSM cathode is plotted as a function of deposition time. As shown in Fig. 4.25, the film growth rate is strongly dependent on the deposition conditions and is drastically increasing with increasing the solution concentration, deposition temperature and the solution flow rate. The trend is similar to what was observed in the first graded sample; however, the difference between the overall thickness (~ 50 μm) of the second graded film and the first one is associated with rotation of the substrate during spraying. As it was mentioned before, films of constant thickness can be fabricated if the spray flow sweeps the whole surface uniformly.

4. 4. Electrical Conductivity of the Gradient Porous LSM Film

Basically, high electrical conductivity of the LSM cathode at high temperatures results in lower ohmic polarization while the porous microstructure provides path for mass transfer through the cathode microstructure making to the low cathodic polarization possible [73,74]. However, creating a balance between these two requirements is desirable in processing cathode microstructures for IT-SOFCs. Thus, it is important to know that the morphological changes in the microstructure have not resulted in significant drop in electrical conductivity of the cathode film.

To study the effect of gradient porous microstructure with columnar morphology on the charge transfer property, the electrical conductivity of the gradient porous LSM cathode was measured at intermediate temperature range, i.e., (500-700 °C) and is plotted over the reciprocal of temperature.
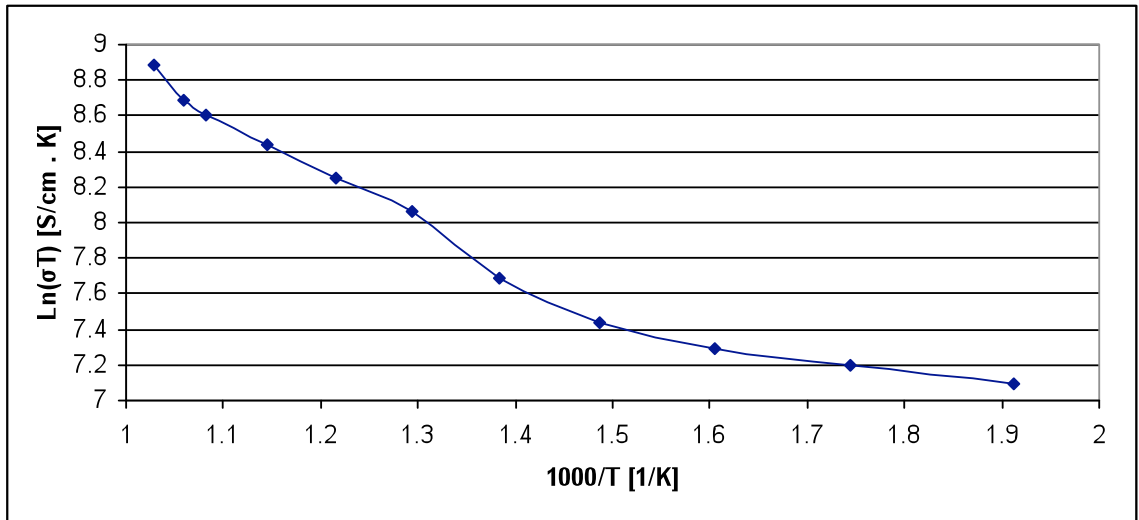

Fig. 4.26 The electrical conductivity of gradient porous LSM film as a function of reciprocal absolute temperature.

Shown in Fig. 4.26, the plot suggests that the conductivity of the gradient porous LSM film is in the acceptable data range required for SOFC cathode. The electrical

conductivity increases with increasing the temperature with lower slope from 250 to 500 °C. The slope changes drastically from 500 to 700 °C showing the highest rate of charge transfer over this temperature range which is the working temperature range for IT-SOFCs. Significant increase is also observed at 700 °C. However, deviation from the linear relation can be associated with the fact that activation energy of the porous film for electron conduction was increased with the increase of temperature.

Fig. 4.27 Comparison of electrical conductivity (Log(σ T)) as a function of reciprocal temperature in air for (a) gradient porous LSM film after heat treatment, (b) LSM film prepared by plasma spraying after heat treatment, and (c) LSM film prepared by screen printing.
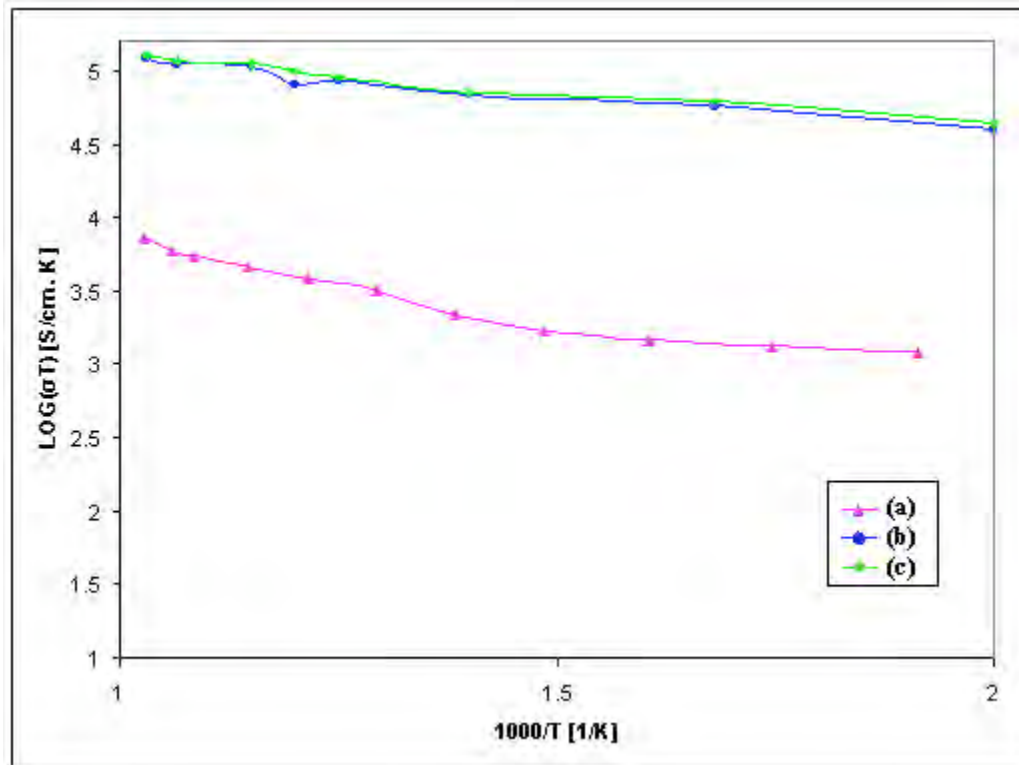
Fig. 4.27 shows comparison of electrical conductivity (Log(σ T)) as a function of reciprocal temperature in air for the gradient porous LSM film after heat treatment, the LSM film prepared by plasma spraying after heat treatment and LSM film prepared by

screen printing. Compared to these processing techniques, the electrical conductivity of the gradient porous LSM film fabricated by spray pyrolysis is nearly the close to that of films prepared by plasma spraying and screen printing [74]. The difference between the conductivity of the gradient porous LSM with the two other LSM films can be attributed to their dissimilar morphology and porosity of the films.

.

CHAPTER 5

CONCLUSIONS AND FUTURE WORK

Gradient porous LSM cathode film was successfully deposited on polycrystalline YSZ electrolyte substrates using multiple-step spray pyrolysis technique. Metal-organic precursors and organic solvent which resulted in a homogeneous crack-free deposition have proven to be more satisfactory than aqueous solution. It was shown that temperature and solution flow rate along with the solution concentration are responsible for the characteristics of the deposited film. Based on the effect of these spray parameters the morphology and porosity of the microstructure was controlled through a 4 step deposition process by changing the deposition temperature in the range of 520-580 °C, and the solution flow rate from 0.73-1.58 ml/min. The resulting porous cathode was consisting of crystalline nanostructured LSM thin film close to the YSZ substrate and gradually porous coarser layers on the surface. Conclusively, modified spray pyrolysis demonstrated great capability to control the microstructure, and particularly porosity of the cathode and is therefore a promising technique for low temperature processing of cathodes with improved microstructural features for being used in IT-SOFCs.

The gradient porous LSM microstructure provides adequate porosity at the top surface for oxygen supply and transport that makes low cathodic polarization possible. The film showed good electrical conductivity between 500-700 °C temperature range after heat treatment.

It is noted that the temperatures at which the as-prepared LSM films transformed to the perovskite phase are significantly below the sintering temperatures required for

traditional methods of film preparation. Thus, running the spray pyrolysis in conditions close to MOCVD revealed that there is the possibility for low-temperature and costly deposition of highly crystalline phase films on large areas for fabrication of SOFCs components without need for high-temperature post-annealing.

REFERENCES

[1]   Chen K, Lu Z, Ai N, Chen X, Hu J, Huang X, et al. Effect of SDC-impregnated LSM cathodes on the performance of anode-supported YSZ films for SOFCs. *Journal of Power Sources*. 2007 **167**: 84-9.

[2]   Li JQ, Xiao P. Fabrication and characterisation of La0.8Sr0.2MnO3/metal interfaces for application in SOFCs. *Journal of the European Ceramic Society*. 2001 **21**: 659-68.

[3]   Wang W, Jiang SP. A mechanistic study on the activation process of (La, Sr)MnO3 electrodes of solid oxide fuel cells. *Solid State Ionics*. 2006 **177**: 1361-9.

[4]   Tsai T, Barnett SA. Effect of LSM-YSZ cathode on thin-electrolyte solid oxide fuel cell performance. *Solid State Ionics*. 1997 **93**: 207-17.

[5]   Sahu DR, Roul BK, Pramanik P, Huang J-L. Synthesis of La0.7Sr0.3MnO3 materials by versatile chemical technique. *Physica B: Condensed Matter*. 2005 **369**: 209-14.

[6]   Daniel J. L. Brett, Alan Atkinson, Nigel P. Brandon, Skinner SJ. Intermediate temperature solid oxide fuel cells. *Chem Soc Rev*. 2008 **37**: 20.

[7]   Swierczek K, Marzec J, Palubiak D, Zajac W, Molenda J. LFN and LSCFN perovskites -- structure and transport properties. *Solid State Ionics*. 2006 **177**: 1811-7.

[8]   Sakito Y, Hirano A, Imanishi N, Takeda Y, Yamamoto O, Liu Y. Silver infiltrated La0.6Sr0.4Co0.2Fe0.8O3 cathodes for intermediate temperature solid oxide fuel cells. *Journal of Power Sources*. 2008 **182**: 476-81.

[9]   Li S, Lü Z, Wei B, Huang X, Miao J, Liu Z, et al. Performances of Ba0.5Sr0.5Co0.6Fe0.4O3-[delta]-Ce0.8Sm0.2O1.9 composite cathode materials for IT-SOFC. *Journal of Alloys and Compounds*. 2008 **448**: 116-21.

[10]   Lee KT, Manthiram A. Synthesis and characterization of Nd0.6Sr0.4Co1-yMnyO3-[delta] (0 <= y <= 1.0) cathodes for intermediate temperature solid oxide fuel cells. *Journal of Power Sources*. 2006 **158**: 1202-8.

[11]   Xia C, Rauch W, Chen F, Liu M. Sm0.5Sr0.5CoO3 cathodes for low-temperature SOFCs. *Solid State Ionics*. 2002 **149**: 11-9.

[12]   Wei Zhou ZS, Ran Ran, Hongxia Gu, Wanqin Jin, Nanping Xu. LSCF Nanopowder from Cellulose–Glycine-Nitrate Process and its Application in

Intermediate-Temperature Solid-Oxide Fuel Cells. *Journal of the American Ceramic Society*. 2008 **91**.

[13] Barbucci A, Carpanese P, Cerisola G, Viviani M. Electrochemical investigation of mixed ionic/electronic cathodes for SOFCs. *Solid State Ionics*. 2005 **176**: 1753-8.

[14] Beckel D, Muecke UP, Gyger T, Florey G, Infortuna A, Gauckler LJ. Electrochemical performance of LSCF based thin film cathodes prepared by spray pyrolysis. *Solid State Ionics*. 2007 **178**: 407-15.

[15] Albert Tarancón SJS, Richard J. Chater, F. Hernández-Ramírez and John A. Kilner. Layered perovskites as promising cathodes for intermediate temperature solid oxide fuel cells *Journal of Materials Chemistry*. 2007 **17**: 6.

[16] Tarancón A, Marrero-López D, Peña-Martínez J, Ruiz-Morales JC, Núñez P. Effect of phase transition on high-temperature electrical properties of GdBaCo2O5 + x layered perovskite. *Solid State Ionics*. 2008 **179**: 611-8.

[17] Zhou Q, He T, Ji Y. SmBaCo2O5+x double-perovskite structure cathode material for intermediate-temperature solid-oxide fuel cells. *Journal of Power Sources*. **In Press, Corrected Proof**.

[18] Zhao F, Peng R, Xia C. LSC-based electrode with high durability for IT-SOFCs. *Fuel Cells Bulletin*. 2008 **2008**: 12-6.

[19] Ji Y, Kilner JA, Carolan MF. Electrical properties and oxygen diffusion in yttria-stabilised zirconia (YSZ)-La0.8Sr0.2MnO3±[delta] (LSM) composites. *Solid State Ionics*. 2005 **176**: 937-43.

[20] Bebelis S, Kotsionopoulos N, Mai A, Rutenbeck D, Tietz F. Electrochemical characterization of mixed conducting and composite SOFC cathodes. *Solid State Ionics*. 2006 **177**: 1843-8.

[21] Princivalle A, Djurado E. Nanostructured LSM/YSZ composite cathodes for IT-SOFC: A comprehensive microstructural study by electrostatic spray deposition. *Solid State Ionics*. **In Press, Corrected Proof**.

[22] Suzuki T, Awano M, Jasinski P, Petrovsky V, Anderson HU. Composite (La, Sr)MnO3-YSZ cathode for SOFC. *Solid State Ionics*. 2006 **177**: 2071-4.

[23] Backhaus-Ricoult M. Interface chemistry in LSM-YSZ composite SOFC cathodes. *Solid State Ionics*. 2006 **177**: 2195-200.

[24] Ruiz-Morales JC, Canales-Vazquez J, Ballesteros-Perez B, Pena-Martinez J, Marrero-Lopez D, Irvine JTS, et al. LSCM-(YSZ-CGO) composites as improved symmetrical electrodes for solid oxide fuel cells. *Journal of the European Ceramic Society*. 2007 **In Press, Corrected Proof**.

[25] Zhao F, Wang Z, Liu M, Zhang L, Xia C, Chen F. Novel nano-network cathodes for solid oxide fuel cells. *Journal of Power Sources*. 2008 **185**: 13-8.

[26] Liu Y, Compson C, Liu M. Nanostructured and functionally graded cathodes for intermediate temperature solid oxide fuel cells. *Journal of Power Sources*. 2004 **138**: 194-8.

[27] Wenquan Gong, Srikanth Gopalan, Pa UB. Materials system for intermediate temperature (600-800°C) solid oxide fuel cells based on doped lanthanum-gallate electrolyte. *Electrochemical Society Proceedings*. 2005-07 **2005-07**: 419-28.

[28] D.S. Li, G. Saheli, M. Khaleel, Garmestani H. Quantitative prediction of effective conductivity in anisotropic heterogeneous media using two-point correlation functions. *Computational Materials Science*. 2006 **38**.

[29]   D.S. Li, G. Saheli, M. Khaleel, Garmestani H. Microstructure optimization in fuel cell electrodes using materials design. *CMC*. 2006 **4**.

[30]   G. SAHELI, H. GARMESTANI, ADAMS BL. Microstructure design of a two phase composite using two-point correlation functions. *Journal of Computer-Aided Materials Design*. 2004 **11**: 103-15.

[31]   Deseure J, Dessemond L, Bultel Y, Siebert E. Modelling of a SOFC graded cathode. *Journal of the European Ceramic Society*. 2005 **25**: 2673-6.

[32]   Greene ES, Chiu WKS, Medeiros MG. Mass transfer in graded microstructure solid oxide fuel cell electrodes. *Journal of Power Sources*. 2006 **161**: 225-31.

[33]   Ni M, Leung MKH, Leung DYC. Micro-Scale Modeling of a Functionally Graded Ni-YSZ Anode. *Chem Eng Technol*. 2007 **30**: 5.

[34]   J. DESEURE, Y. BULTEL, L. DESSEMOND, SIEBERT E, OZIL P. Modelling the porous cathode of a SOFC: oxygen reduction mechanism effect. *Journal of Applied Electrochemistry*. 2007 **37**.

[35]   Holtappels P, Bagger C. Fabrication and performance of advanced multi-layer SOFC cathodes. *Journal of the European Ceramic Society*. 2002 **22**: 41-8.

[36]   Hart NT, Brandon NP, Day MJ, Lapeña-Rey N. Functionally graded composite cathodes for solid oxide fuel cells. *Journal of Power Sources*. 2002 **106**: 42-50.

[37]   J. Deseure, Y. Bultel, L. C. R. Schneider, L. Dessemond, Martin C. Micromodeling of Functionally Graded SOFC Cathodes. *Journal of The Electrochemical Society*. 2007 **154**.

[38]   J. Deseure, Y. Bultel, L. Dessemond, Siebert. E. Theoretical optimisation of a SOFC composite cathode. *Electrochimica Acta*. 2005 **50**: 2037-46.

[39]   Tanner CW, Fung K-Z, Virkar AV. The Effect of Porous Composite Electrode Structure on Solid Oxide Fuel Cell Performance. *Journal of The Electrochemical Society*. 1997 **144**: 21-30.

[40]   Choy KL, Charojrochkul S, Steele BCH. Fabrication of cathode for solid oxide fuel cells using flame assisted vapour deposition technique. *Solid State Ionics*. 1997 **96**: 49-54.

[41]   Chiba R, Yoshimura F, Sakurai Y, Tabata Y, Arakawa M. A study of cathode materials for intermediate temperature SOFCs prepared by the sol-gel method. *Solid State Ionics*. 2004 **175**: 23-7.

[42]   Subramania A, Saradha T, Muzhumathi S. Synthesis of nano-crystalline (Ba0.5Sr0.5)Co0.8Fe0.2O3-[delta] cathode material by a novel sol-gel thermolysis process for IT-SOFCs. *Journal of Power Sources*. 2007 **165**: 728-32.

[43]   Yoon SP, Han J, Nam SW, Lim T-H, Oh I-H, Hong S-A, et al. Performance of anode-supported solid oxide fuel cell with La0.85Sr0.15MnO3 cathode modified by sol-gel coating technique. *Journal of Power Sources*. 2002 **106**: 160-6.

[44]   Cheng CS, Zhang L, Zhang YJ, Jiang SP. Synthesis of LaCoO3 nano-powders by aqueous gel-casting for intermediate temperature solid oxide fuel cells. *Solid State Ionics*. 2008 **179**: 282-9.

[45]   Montinaro D, Sglavo VM, Bertoldi M, Zandonella T, Aricò A, Lo Faro M, et al. Tape casting fabrication and co-sintering of solid oxide "half cells" with a cathode-electrolyte porous interface. *Solid State Ionics*. 2006 **177**: 2093-7.

[46]   Caillol N, Pijolat M, Siebert E. Investigation of chemisorbed oxygen, surface segregation and effect of post-treatments on La0.8Sr0.2MnO3 powder and screen-

printed layers for solid oxide fuel cell cathodes. *Applied Surface Science*. 2007 **253**: 4641-8.

[47]   Van herle J, Ihringer R, Vasquez Cavieres R, Constantin L, Bucheli O. Anode supported solid oxide fuel cells with screen-printed cathodes. *Journal of the European Ceramic Society*. 2001 **21**: 1855-9.

[48]   Zhang Y, Liu J, Huang X, Lu Z, Su W. Low temperature solid oxide fuel cell with Ba0.5Sr0.5Co0.8Fe0.2O3 cathode prepared by screen printing. *Solid State Ionics*. 2008 **179**: 250-5.

[49]   Will J, Mitterdorfer A, Kleinlogel C, Perednis D, Gauckler LJ. Fabrication of thin electrolytes for second-generation solid oxide fuel cells. *Solid State Ionics*. 2000 **131**: 79-96.

[50]   Perednis D, Wilhelm O, Pratsinis SE, Gauckler LJ. Morphology and deposition of thin yttria-stabilized zirconia films using spray pyrolysis. *Thin Solid Films*. 2005 **474**: 84-95.

[51]   Kumar A, Devi PS, Maiti HS. Effect of metal ion concentration on synthesis and properties of La0.84Sr0.16MnO3 cathode material. *Journal of Power Sources*. 2006 **161**: 79-86.

[52]   Mench MM. Fuel Cell Engines. 2008.

[53]   Stover D, Buchkremer HP, Uhlenbruck S. Processing and properties of the ceramic conductive multilayer device solid oxide fuel cell (SOFC). *Ceramics International*. 2004 **30**: 1107-13.

[54]   Prabhakar Singh, Minh NQ. Solid Oxide Fuel Cells: Technology Status. *The International Journal of Applied Ceramic Technology*. 2004 **1**: 10.

[55]   Minh NQ. Solid oxide fuel cell technology--features and applications. *Solid State Ionics*. 2004 **174**: 271-7.

[56]   N. T. Hart NPB, M. J. Day and J. E. Shemilt Functionally graded cathodes for solid oxide fuel cells. *Journal of Materials Science*. 2001 **36**: 8.

[57]   Zha S, Zhang Y, Liu M. Functionally graded cathodes fabricated by sol-gel/slurry coating for honeycomb SOFCs. *Solid State Ionics*. 2005 **176**: 25-31.

[58]   Ye F, Wang Z, Weng W, Cheng K, Song C, Du P, et al. Spin-coating derived LSM-SDC films with uniform pore structure. *Thin Solid Films*. 2008 **516**: 5206-9.

[59]   Piao J, Sun K, Zhang N, Xu S. A study of process parameters of LSM and LSM-YSZ composite cathode films prepared by screen-printing. *Journal of Power Sources*. 2008 **175**: 288-95.

[60]   Beckel D, Bieberle-Hütter A, Harvey A, Infortuna A, Muecke UP, Prestat M, et al. Thin films for micro solid oxide fuel cells. *Journal of Power Sources*. 2007 **173**: 325-45.

[61]   D. Perednis. Thin Film Deposition by Spray Pyrolysis and the Application in Solid Oxide Fuel Cells. *PhD Thesis, Swiss Federal Institute of Technology, Zurich*. 2003.

[62]   Madler L. Liquid-fed Aerosol Reactors for One-step Synthesis of Nano-structured Particles. *Kona*. 2004 **22**.

[63]   Beckel D, Dubach A, Studart R, Gauckler LJ. Spray pyrolysis of La0.6Sr0.4Co0.2Fe0.8O3-δ thin film cathodes. *Journal of electroceramics*. 2006 **16**.

[64]   Viguie JC, Spitz J. Chemical Vapor Deposition at Low Temperatures. *Journal of The Electrochemical Society*. 1975 **122**: 585-8.

[65]   Gary L. Messing, Shi-Chang Zhang, Jayanthi GV. Ceramic Powder Synthesis by Spray Pyrolysis

J Am Cer Soc. 1993 **76**.

[66]   Perednis D, Gauckler LJ. Solid oxide fuel cells with electrolytes prepared via spray pyrolysis. *Solid State Ionics*. 2004 **166**: 229-39.

[67]   Chen CH, Emond MHJ, Kelder EM, Meester B, Schoonman J. ELECTROSTATIC SOL-SPRAY DEPOSITION OF NANOSTRUCTURED CERAMIC THIN FILMS. *Journal of Aerosol Science*. 1999 **30**: 959-67.

[68]   Charojrochkul S, Choy KL, Steele BCH. Flame assisted vapour deposition of cathode for solid oxide fuel cells. 1. Microstructure control from processing parameters. *Journal of the European Ceramic Society*. 2004 **24**: 2515-26.

[69]   Abrutis A, Teiserskis A, Garcia G, Kubilius V, Saltyte Z, Salciunas Z, et al. Preparation of dense, ultra-thin MIEC ceramic membranes by atmospheric spray-pyrolysis technique. *Journal of Membrane Science*. 2004 **240**: 113-22.

[70]   Kang HS, Kang YC, Koo HY, Ju SH, Kim DY, Hong SK, et al. Nano-sized ceria particles prepared by spray pyrolysis using polymeric precursor solution. *Materials Science and Engineering: B*. 2006 **127**: 99-104.

[71]   Song HS, Kim WH, Hyun SH, Moon J, Kim J, Lee H-W. Effect of starting particulate materials on microstructure and cathodic performance of nanoporous LSM-YSZ composite cathodes. *Journal of Power Sources*. 2007 **167**: 258-64.

[72]   Belzner A, Gur TM, Huggins RA. Oxygen chemical diffusion in strontium doped lanthanum manganites. *Solid State Ionics*. 1992 **57**: 327-37.

[73]   Li C-J, Li C-X, Wang M. Effect of spray parameters on the electrical conductivity of plasma-sprayed La1-xSrxMnO3 coating for the cathode of SOFCs. *Surface and Coatings Technology*. 2005 **198**: 278-82.

[74]   Huaiwen Nie, Wenhua Huang, Ting-Lian Wen, Hengyong Tu, Zhan Z. LSM cathodes for SOFC prepared by plasma spraying. *JOURNAL OF MATERIALS SCIENCE LETTERS*. 2002 **21**.